UNIVERSITÀ POLITECNICA DELLE MARCHE
Facoltà di Medicina e Chirurgia
Dipartimento di Scienze Biomediche e Sanità Pubblica
Corso di Dottorato in Biomedical Sciences
XXXVII Ciclo

Metabolism and Pharmacological Characterization at μ-, κ-, and δ- Opioid Receptors Using a Novel Non-Radioactive Assay of Nitazenes and Methadone-like Synthetic Opioids

Candidata:
Dott.ssa Diletta Berardinelli

Tutor:
Chiar. mo Prof. Francesco Paolo Busardò

Valutatori:
Chiar.mo Prof. Pascal Kintz
Chiar.mo Prof. Oscar Garcia

Coordinatore del Corso di Dottorato:
Chiar.mo Prof. Francesco Paolo Busardò

A.A. 2023-2024

Index

1.1. New Psychoactive Substances 3

1.2. Novel synthetic opioids and the rise of nitazenes 5

1.3. Opioid receptor system: μ-, κ-, and δ-opioid receptors 10

2. *In vitro* and *in vivo* metabolism of a panel of Nitazenes 14

2.1. Materials and methods 14

2.1.1. Chemicals and reagents 14

2.1.2. *In silico* metabolite prediction 15

2.1.3. Human hepatocyte incubation 16

2.1.4. pHLM assay 17

2.1.5. Authentic human samples 18

2.1.6. Samples preparation 18

2.1.7. Identification of Metabolites using LC-HRMS/MS 20

2.1.8. Instrumental conditions 20

2.1.8.1. Dipyanone LC-HRMS/MS settings 20

2.1.8.2. Etonitazepipne LC-HRMS/MS setting 25

2.1.8.3. Protonitazepyne and Metonitazepyne LC-HRMS/MS setting 31

2.1.9. Data mining 39

3. μ-, κ-, and δ- Opioid receptor pharmacological characterization 40

3.1. Materials and methods 40

3.1.1. Chemicals and reagents 40

3.1.2. Instrumental conditions 41

3.1.2.1. HTRF-based GTP Gi binding assay 41

3.1.3. Data analysis and statistical methods 42

4. Results 43

4.1. Metabolites identification in human hepatocyte & pHLM 43

4.1.1. Etonitazepipne metabolites identification in pHLM 43

4.1.2. Etonitazepipne fragmentation pattern 48

4.1.2.1. *O*-Deethylation 49

4.1.2.2. *O*-Deethylation and ketone formation (or *N*-oxidation) 50

4.1.2.3. Hydroxylation 51

4.1.3. *In vivo* Metabolites Identification 52

4.1.4. Dipyanone metabolites identification in human hepatocytes 53

4.1.5. Dipyanone Fragmentation Pattern 58

4.1.5.1. Pyrrolidine ring opening and cyclisation 59

4.1.5.2. *In vivo* Metabolites Identification 62

4.1.6. Protonitazepyne & Metonitazepyne metabolites identification in human hepatocytes 63
4.1.7. Protonitazepyne and Metonitazepyne Fragmentation Pattern 69
4.1.7.1. *N*-dealkylation to butanoic acid 69
4.1.7.2. Oxidation 70
4.1.7.3. Hydroxylation 70
4.1.7.4. *O*-dealklation and *O*-glucuronidation 71
4.1.8. *In vivo* Metabolite Identification 74
4.2. MOR, KOR, and DOR *in vitro* activation profiles 74
4.2.1. Etonitazepipne 74
4.2.2. Dipyanone 75
4.2.3. Protonitazepyne and metonitazepyne 75
5. Discussion 79
5.1. NSO metabolic profiling 79
5.1.1. Etonitazepipne metabolism 79
5.1.2. Dipyanone metabolism 80
5.1.3. Protonitazepyne and Metonitazepyne metabolism 81
5.2. Pharmacological properties of nitazenes at opioid receptors 82
5.2.1. Etonitazepipne opioid receptors' activation 82
5.2.2. Dipyanone opioid receptors' activation 83
5.2.3. Protonitazepyne and metonitazepyne opioid receptors' activation 85
6. Conclusion 87
6.1. Key findings 87
6.3. Limitations and Future perspectives 89
7. Bibliography 90

1. Introduction

1.1. New Psychoactive Substances

New Psychoactive Substances (NPS) are a heterogeneous and complex group of substances designed to mimic the psychoactive effects of licensed medicines or controlled substances worldwide. These substances are commonly referred as "synthetic drugs", "designer drugs", "bath salts", "research chemicals", and "legal drugs". Most of these substances are sold as "legal" substitutes for illicit drugs, while others are intended for those who want to experience their possible new effects.

Every year, several NPSs with minor structural modifications emerge onto the drug market to circumvent the legislation and analytical detection, and for this reason they are hardly and slowly subjected to international control. The United Nations Office on Drugs and Crime (UNODC) defines NPSs as "*substances of abuse, in pure form or in a preparation, which are not controlled by the 1961 Single Convention on Narcotic Drugs or the 1971 Convention on Drugs psychotropic, but which may pose a threat to public health*" (1).

Therefore, the term NPS does not only refer to illegal substances synthesized for the first time, but also to drugs of natural origin or substances that have already existed for years or decades. For example, legal drugs, such as candidate medicines that did not reach the pharmaceutical market due to excessive side effects or limited pharmacological benefits, may enter the illegal market, even many years after their first synthesis (2).

According to the World Drug Report, in 2022, 566 distinct NPSs were identified on the market (Fig 1). Although the number of synthetic opioids, such as fentanyl analogues, significantly increased between 2010 and 2020, except for 2023, where it was reported a sharply decline, reports of nitazenes, continued to rise (2).

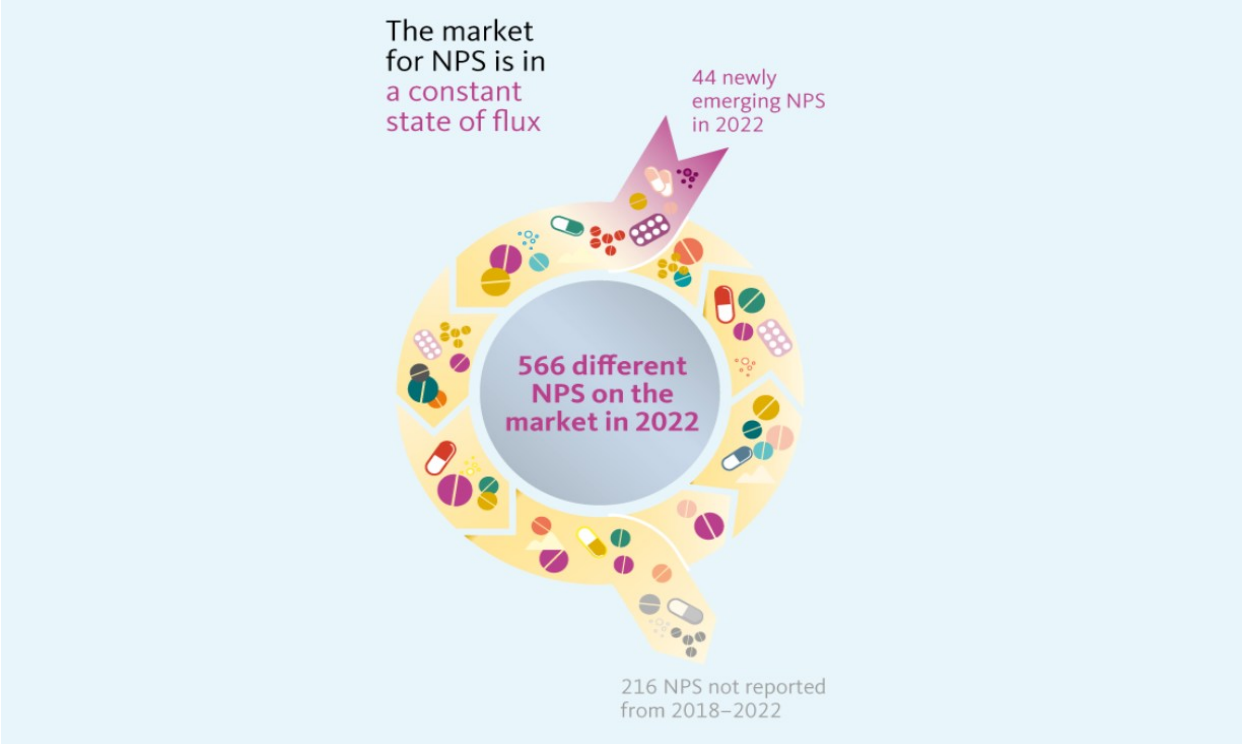


Figure 1: Number of NPS detected in the global market in 2022. Source, Early Warning Advisor on New Psychoactive Substances

Novel Synthetic Opioids (NSOs) represent a wide class of NPSs producing analgesic and anesthetic effects, similar to traditional opioids such as morphine and heroin. Opiates are the naturally occurring alkaloids in the opium poppy and include morphine, codeine, and thebaine; their semisynthetic derivatives include heroin, hydrocodone, oxycodone, and buprenorphine. The opioid class also includes several synthetic or pharmaceutical opioids, such as methadone, pethidine, tramadol, and fentanyl. Synthetic opioids are μ, δ, and κ opioid receptor agonists (MOR, KOR and DOR), depressing respiration, increasing sensations of pleasure, and blocking

the nervous system's pain messages. They are typically used as heroin substitutes due to low cost and to circumvent legislation and analytical detection. Side effects include extreme happiness, nausea, constipation, sedation, and respiratory arrest (3). In fact, minimal doses are enough to produce even lethal effects, and small quantities can correspond to thousands of doses. Recently, synthetic opioids, led by fentanyl and analogues, have caused a spike in intoxication and thousands of overdose fatalities in North America, upsetting the traditional demographics of opioid-related overdoses (4).

Moreover, as happened with other NPS classes, between 2008 and 2018, the opioid market is increasing its variety, with a consequently diffusion of NSOs involving fentanyl derivatives, which are now under the international legislation control. As a result, the balance has recently shifted toward non-fentanyl NPSs (5,6).

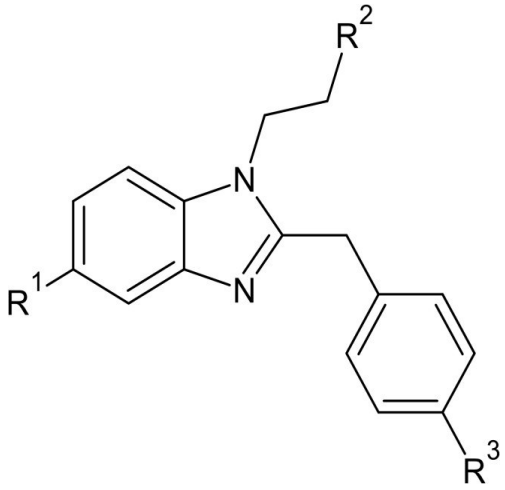
1.2. Novel synthetic opioids and the rise of nitazenes

Over the past decade, the opioid crisis has been dominated by fentanyl and its analogues after its scheduling first in the United States (US) in 2018 and in China in 2019, alternative NSOs have increasingly appeared in the illicit drug market (7,8). Among these, a class of 2-benzylbenzimidazole analogs, also known as nitazenes, have raised significant public health concerns due to their potent effects and potential to cause fatal overdoses. Nitazenes, also called 2-benzylbenzimidazole, were first synthesized in the 1957 by CIBA Aktiengesellschaft Pharmaceuticals as

potential analgesic drugs, however due to their side effects and addiction risks they were never marketed (9,10).

Several studies in animals and humans demonstrated that nitazenes are selective MOR agonists with antinociceptive properties similar to those of morphine. Nausea, fatigue, decreased consciousness, cyanosis, and vomiting are common NSO-related side effects, and respiratory depression may occur, leading to coma and death (7,11). Since their first appearance in 2019, nitazenes have increasingly emerged in the illicit drug market, raising significant public health concerns due to their extreme potency and associated risks. From 2019 to 2024, several analogues of nitazenes have been identified, each contributing to the escalating opioid crisis (7,12).

The main subclasses of nitazenes include etonitazene, isotonitazene, and metonitazene, which were among the first compounds to gain attention for their high potency, exceeding that of fentanyl. Subsequently, additional analogues such as protonitazene, butonitazene, and flunitazene were identified, further expanding the diversity of these compounds. Each of these analogues exhibits unique pharmacological properties but shares potent activation at μ-opioid receptor. More recently, compounds like N-pyrrolidino and N-piperidinyl nitazenes(such as protonitazepyne, metonitazepyne and etonitazepipne) and other novel derivatives (such as 5-Methyletodesnitazene or Ethyleneoxynitazene) have emerged, demonstrating how clandestine laboratory continually modify these molecules to evade detection and enhance their psychoactive effects (13) (Fig 2).



	R^1	R^2	R^3
Isotonitazene	$-NO_2$	$-C_4H_{10}N$	$-OCH(CH_3)_2$
Etodesnitazene	-H	$-C_4H_{10}N$	$-OC_2H_5$
Metodesnitazene	-H	$-C_4H_{10}N$	$-OCH_3$
Metonitazene	$-NO_2$	$-C_4H_{10}N$	$-OCH_3$
Etonitazene	$-NO_2$	$-C_4H_{10}N$	$-OC_2H_5$
Protonitazene	$-NO_2$	$-C_4H_{10}N$	$-OC_3H_7$
Clonitazene	$-NO_2$	$-C_4H_{10}N$	-Cl
Etonitazepipne	$-NO_2$	$-C_5H_{10}N$	$-OC_2H_5$
Etonitazepyne	$-NO_2$	$-C_4H_8N$	$-OC_2H_5$
Protonitazepyne	$-NO_2$	$-C_4H_8N$	$-OC_3H_7$
Metonitazepyne	$-NO_2$	$-C_4H_8N$	$-OCH_3$
5-Methyletodesnitazene	$-CH_3$	$-C_4H_{10}N$	$-OC_2H_5$
Ethyleneoxynitazene	$-NO_2$	$-C_4H_{10}N$	$-OC_3H_6$

Figure 2: Generic structure of Nitazenes and possible side chain modifications

In 2023, the EU Early Warning System recorded NSOs, six of which belonged to the highly potent group of nitazenes. This represents the largest number of nitazenes opioids ever reported in a single year. Since 2019, nitazenes opioids have been detected in at least 20 EU member states. Their increasing diffusion appears to coincide with control measures that aim at limiting the availability of fentanyl derivatives (13) (Fig 3).

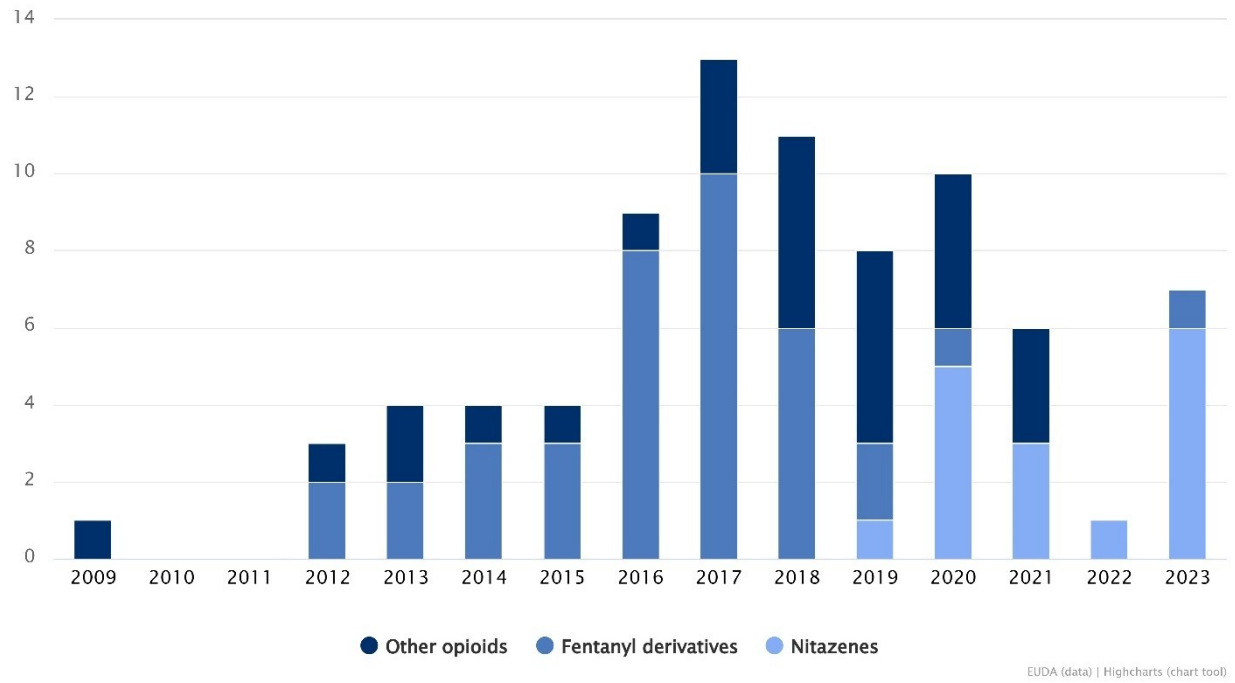


Figure 3: Number of new opioids reported for the first time to the EU Early Warning System. 2009-2023. Source: European Drug Report 2024

Although limited data are available, reports indicate these compounds may share similar pharmacological profiles with other nitazenes, such as increased analgesic activity and a significant risk for overdose and respiratory depression.

In addition to nitazenes, another emerging subclass of NSO gaining attention is the diphenylmethylpiperidine derivatives, with dipyanone being a notable example (13,14). Dipyanone belongs to a group of compounds structurally related to methadone, designed originally in the mid-20th century as potential analgesic (14–17). Although initially developed for therapeutic purposes, their high potency and risk of dependency have led to a resurgence in illicit drug markets. Dipyanone, like nitazenes, acts as a MOR agonist, exhibiting strong antinociceptive effects. However, its pharmacological profile also includes severe side effects such as

profound respiratory depression, sedation, and a high likelihood of overdose fatalities (14,15).

From its first detection in Germany in 2021 and subsequent appearance in Slovenia (18), dipyanone has demonstrated how quickly NSO spread across borders, with several related fatalities reported in 2022 and 2023 (Fig 4) (15).

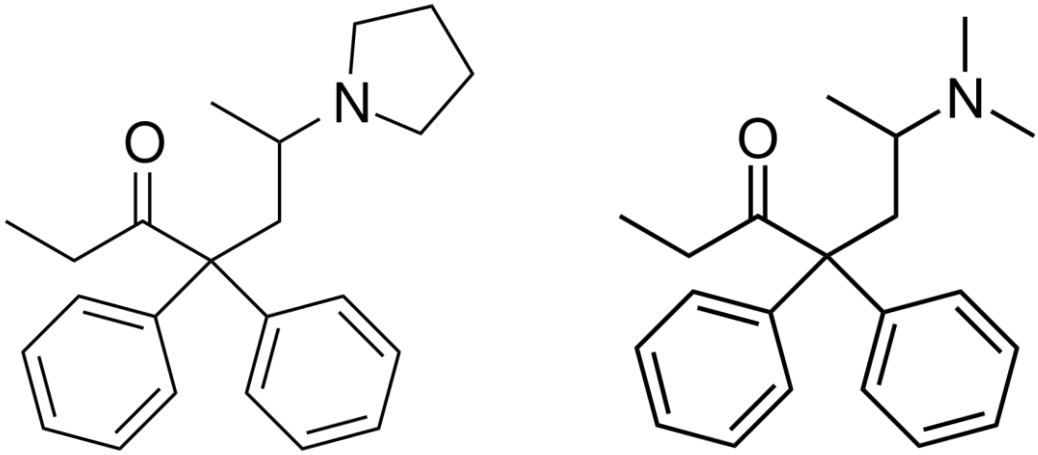


Figure 4: Structure of Dypianone (left) and Methadone (right)

Recently, there have been alarming reports of nitazene-related deaths, particularly in regions like the Baltic states, underscoring the need for further investigation into their pharmacological profiles and the potential for harm (13,19,20).

Furthermore, forensic cases involved in fatal overdoses from North America and the United Kingdom were reported at very low blood concentrations, underscoring their extreme potency and danger (19). This trend highlights the rapid and unpredictable evolution of the New Psychoactive Substances (NPS) market, which often introduces structurally novel compounds in response to regulatory controls.

1.3. Opioid receptor system: μ-, κ-, and δ-opioid receptors

The opioid receptor system, encompassing MOR, KOR, and DOR, plays a central role in the pharmacological and physiological effects of opioids, including NSO (21). These receptors are G-protein-coupled receptors (GPCRs) activated by endogenous peptides such as endorphins, dynorphins, and enkephalins, as well as exogenous drugs. Their activation influences analgesia, mood, and respiratory function, making them key targets in pain management and addiction treatment. MOR is the primary target for analgesic effects but is also responsible for euphoria, respiratory depression, and high addiction potential (22). KOR, activated by dynorphins, modulates stress and aversion, with emerging interest in its therapeutic potential for addiction and mood disorders. DOR, linked to enkephalins, offers neuroprotective and antidepressant-like effects but poses challenges such as seizure risks (22–24) (Fig 5).

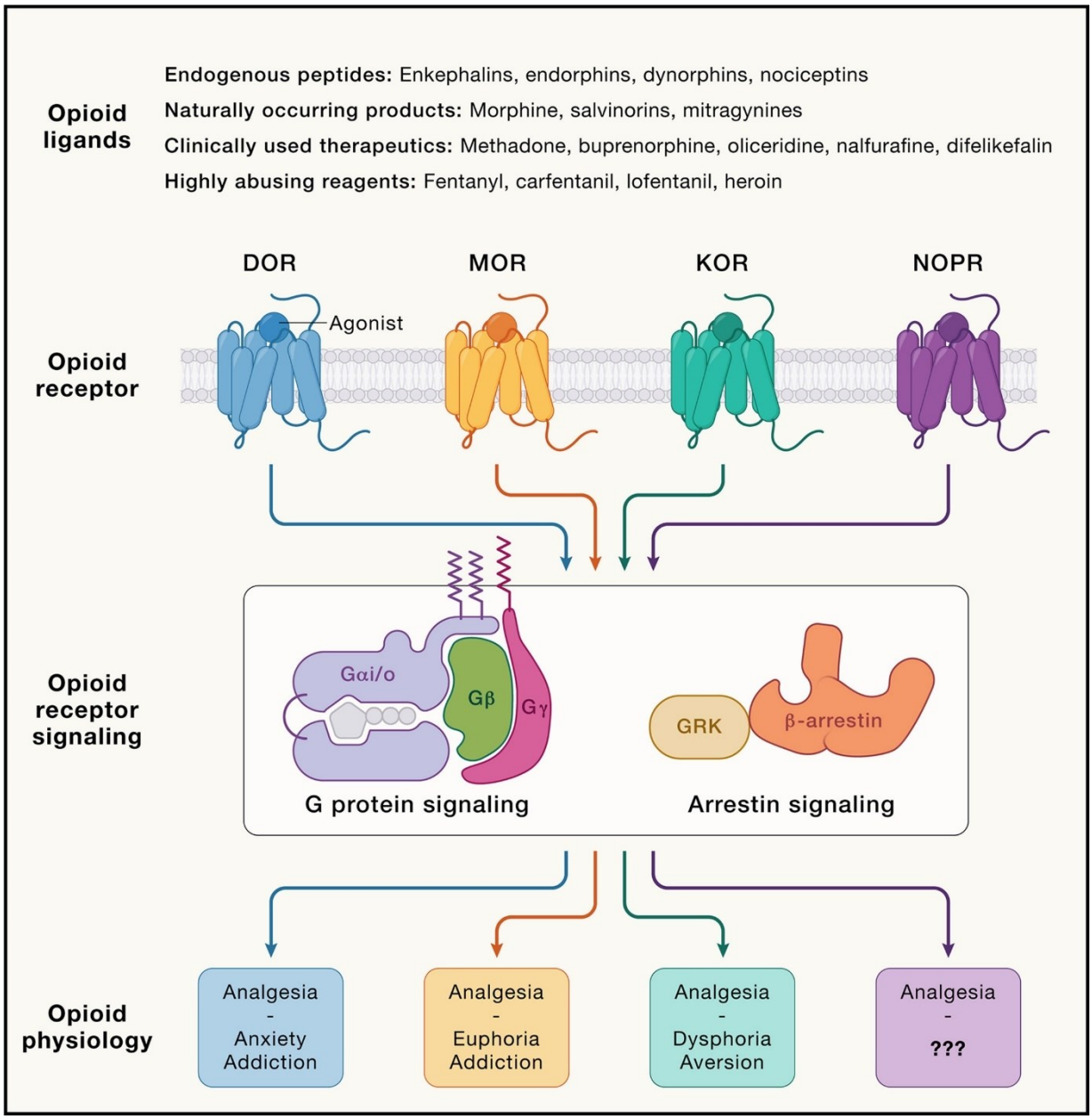


Figure 5: Overview of the action of opioids. Source, Molecular basis of opioid receptor signaling. Cell 2023 186; 24:5203-5219

In the context of NSOs, the pharmacological activity at these receptors is crucial for understanding the potency and toxicity of emerging analogues. Studies of receptor-binding dynamics, signaling pathways, and biased agonism are pivotal for elucidating their therapeutic and adverse effects. Furthermore, detailed receptor studies support the development of high-throughput pharmacological assays, like GTP Gi-binding studies, which are instrumental in assessing novel opioid-receptor

interactions. The adaptability of the opioid receptor system and its interaction with novel compounds underscore the importance of characterizing receptor activity in tandem with metabolic profiling to improve detection and therapeutic strategies for NSOs (25–27) (Fig. 6).

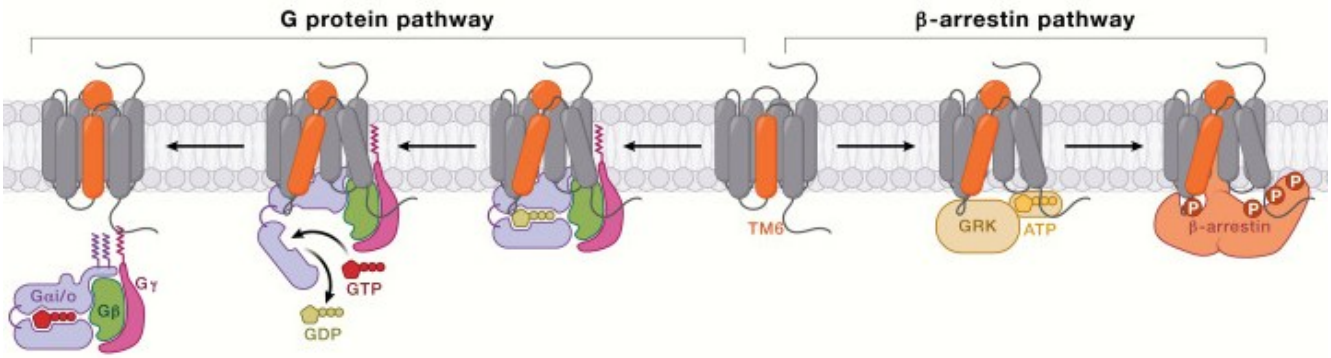


Figure 6: Opioid- and opioid-receptor-mediated signaling pathways. Cell 2023 186; 24:5203-5219

1.4. Aims and Objectives : Metabolite identification and pharmacological characterization

Considering the recent emergence of NSOs onto the illicit drug market and their effects and potencies, law enforcement agencies, medical staff, and toxicology laboratories need to be prepared to cope with this deadly threat. Due to the lack of specific clinical symptoms and autopsy findings, the consumption of NSOs can only be ascertained by the analysis of biological samples, such as blood, urine, and hair, in forensic and clinical cases. However, the detection of the parent drug can be challenging because 1) many NSO are extremely potent and small doses are sufficient to induce recreational effects and toxicity, and 2) they may be quickly transformed into active unknown metabolites (7,28). Therefore, targeting specific metabolite biomarkers of consumption, whose concentrations are usually higher

than those of the parent drug and can be detected over an extended time course, especially in urine, is often preferred to improve detection capabilities in analytical toxicology. The increasing availability of NSOs derivatives and analogues underscores the dynamic and adaptive nature of the synthetic opioid crisis. For this reason, detailed studies on the metabolism and pharmacokinetics of the most recent compound are unknown.

This study aims to address the knowledge gap by investigating the *in vitro* and *in vivo* metabolism of NSO using pooled human hepatocytes, authentic urine and blood samples, and MOR, KOR and DOR activity. In the present study, the metabolism of the four opioids (etonitazepipne, dipyanone, protonitazepyne and metonitazepyne) was studied with 1a) *in vitro* incubations with pooled human hepatocytes of dipyanone, protonitazepyne and metonitazepyne, which contain the full range of phase I and II metabolic enzymes and necessary cofactors and transporters, and provide the natural orientation of membrane enzymes to effectively simulate human *in vivo* metabolism and *in vitro* incubation using pooled human liver microsomes (pHLMs) to identify phase I metabolites of etonitazepipne; 1b) *in vivo* analysis of postmortem real samples of etonitazepipne, dipyanone and protonitazepyne; 2) high-performance liquid chromatography-high-resolution tandem mass spectrometry (LC-HRMS/MS) analysis of incubates, to exhaustively detect the metabolites and capture their HRMS/MS fragmentation pattern in a single analysis with accurate mass capabilities; and 3) software-assisted mining of LC-HRMS/MS raw data, to screen expected and unexpected metabolites with a partially

automated workflow; steps 2) and 3) were supported by *in silico* phase I and phase II metabolite predictions in humans (29).

Moreover, the pharmacology of four compounds was studied through 1) development and optimization of a fast and high-throughput HTRF® based GTP Gi binding assay; 2) analyses through a MultiLabel plate reader; 3) pharmacological and statistical data were obtained through GraphPad Prism Software (v10.4.0) providing a comprehensive understanding of their pharmacological and metabolic profiles.

2. *In vitro* and *in vivo* metabolism of a panel of Nitazenes

2.1. Materials and methods

2.1.1. Chemicals and reagents

Etonitazepipne, dipyanone, protonitazepyne, metonitazepyne, fentanyl, SNC-80, and U-50488 pure standards were bought from Cayman Chemical (Ann Arbor, MI, USA), and diclofenac was purchased from Sigma Aldrich (Milan, Italy). The standards were diluted in methanol at 1 mg/mL and stored at − 20°C until analysis. LC-MS grade methanol, acetonitrile, water, and formic acid. Were supplied by Carlo Erba (Cornaredo, Italy). Williams' medium E (WME), HEPES buffer (2-[4-(2-hydroxyethyl)-1- piperazinyl]ethanesulfonic acid), and l-Glutamine were obtained from Sigma Aldrich. Supplemented Williams' Medium E (SWM) was prepared by dissolving HEPES and l-Glutamine at 2 and 20 mmol/L, respectively, in WME. The solution was stored at 4°C until incubation. Thawing medium, 0.4%

trypan blue, and ten-donor-pooled cryopreserved human hepatocytes (HEP) were purchased from Lonza (Basel, Switzerland). μ, κ and δ human opioid receptor membrane, 96-well plate and the GTP Gi Binding assay Kit were purchased from Revvity (Italy). Carl Roth (Karlsruhe, Germany) provided the following solvents and reagents: formic acid (Rotipuran® ≥98 %, p.a.), sodium hydroxide (≥99 %, p.a., pellets) and potassium hydrogen phosphate (≥99 %, p.a.). pHLM (50 donors, 20 mg/mL protein in 250 mM sucrose), NADPH regenerating Solutions A and B (reductase activity 0.43 μmol/ min × mL) and potassium phosphate buffer 0.5 mol/L (pH 7.5) were purchased from Corning (New York, USA). NADPH regenerating Solution A composition was as follows: 26 mM NADP+, 66 mM glucose 6 phosphate and 66 mM MgCl2 in water. NADPH regenerating Solution B consisted of 40 U/mL glucose 6-phosphate dehydrogenase in 5 mM sodium citrate.

2.1.2. *In silico* metabolite prediction

Etonitazepipne, dipyanone, protonitazepyne and metonitazepyne phase I and phase II human metabolites were predicted using GLORYx, an open-access software featured on a web portal from the University of Hamburg, Germany (https://nerdd.zbh.unihamburg.de/). GLORYx uses reaction rule sets to generate the structures of putative metabolites, combined with predicted sites of metabolism to score and rank the metabolites; the site of metabolism is predicted through another open access software, FAME 3, using a collection of machine learning models (30,31). The “Phase 1 and Phase 2 metabolism” mode was selected to predict first-

generation (one metabolic transformation) phase I and phase II metabolites. First-generation metabolites with a score equal or higher than 50% were reprocessed, after generating their SMILES through ChemSketch, to predict second-generation metabolites (two metabolic transformations). The score of the second-generation metabolites was multiplied by the score of the corresponding first-generation metabolite to calculate a "modified score". The accurate masses of predicted metabolites were compiled in an inclusion list for LC-HRMS/MS analysis to prioritize the fragmentation of specific targets. All predicted metabolic reactions and combinations were included in the list of possible transformations for data mining.

2.1.3. Human hepatocyte incubation

Hepatocytes were thawed at 37°C in a thermostatic water bath for about 90-120 s and gently mixed in 50 mL TM at 37°C in a 50 mL polypropylene conical tube. The tube was centrifuged at 100*g* for 5 min at room temperature and the supernatant was discarded, while the cells were resuspended in 50 mL sWME at 37°C. A second centrifugation at 100*g* for 5 min was performed, and the supernatant was discarded, while the cells were resuspended in 2 mL sWME at 37°C. Cell viability was assessed through the trypan blue exclusion staining method (Figure 6), and the sWME volume was adjusted to 2×106 viable cells/mL.

Incubations were prepared in sterile 24-well culture plates with 250 µL hepatocyte suspension at 2×10^6 viable cells/mL in sWME at 37°C and 250 µL dipyanone,

protonitazepyne and metonitazepyne at 20 μmol/L in sWME at 37°C; each analogue was incubated separately. The plates were stored in an incubator previously set at 37°C (Argo Lab; Carpi, Italy), and gently mixed every 30 min. Metabolic reactions were stopped with 500 μL ice-cold acetonitrile after 3 h. The samples were transferred into microtubes, centrifuged for 10 min, 15,000*g*, at room temperature, and stored at -80°C until analysis.

All the incubations were performed alongside with diclofenac, which was used as a positive control to ensure proper metabolic activity of the hepatocytes. In addition, negative controls were used to rule out non-metabolic reactions and other interferences.

2.1.4. pHLM assay

Etonitazepipne pHLM incubation assay was performed using previous published protocol to identify phase I metabolites using pooled human liver microsomes (32,33). Total assay volume (100 μL) consisted of phosphate buffer (0.5 M), NADPH regenerating system: solution A (NADP+ and glucose-6-phosphate) and B (glucose-6-phosphate dehydrogenase), superoxide dismutase (200 units/mL), deionized water, pHLM (1 mg/mL), and etonitazepipne (final concentration: 10 μg/mL in methanol). Incubation was performed for 120 min at 37 °C. Incubations with control without pHLM (negative) and drug substrate (blank) were processed simultaneously. Incubations were quenched adding 100 μL ice-cold ACN.

2.1.5. Authentic human samples

Postmortem biological samples from four distinct cases in Germany were analysed to investigate the presence and effects of novel synthetic opioids. The cases involved the substances etonitazepipne (Case #1), dipyanone (Case #2a and 2b), and metonitazepyne (Case #3).

2.1.6. Samples preparation

Following previously published protocols (29,33), incubates from human hepatocytes were thawed at room temperature and centrifuged at 15,000*g* for 10 min, at room temperature. A volume of 100 µL supernatant was mixed with 100 µL acetonitrile, then centrifuged again at 15,000*g* for 10 min, at room temperature. The supernatants were dried in conical glass tubes at 37°C under nitrogen and reconstituted with 150 µL mobile phases A and B (A:B; 90:10, v/v). After centrifugation at 15,000*g* for 10 min, at room temperature, the supernatants were transferred into autosampler vials with a glass insert, and 15 µL was injected onto the chromatographic system.

As previously reported(32,33), incubates from pHLMs were thawed at room temperature and centrifuged at 15,000*g* for 10 min, at room temperature. A volume of 100 µL supernatant was mixed with 50 µL of ammonium formate (10 mol/L) was added and samples were centrifuged at 13,680 g for 4 min. The organic phase was transferred into a vial and evaporated to dryness under a nitrogen stream at 40 °C, and reconstituted in 100 µL mobile phase A (0.1 % formic acid in water): mobile

phase B (0.1 % formic acid in acetonitrile), 90:10, v/v. All experiments were performed in triplicates. Authentic human samples were thawed at room temperature, and 100 µL was mixed with 200 µL acetonitrile and centrifuged for 10 min, 15,000g, at room temperature. The supernatants were evaporated to dryness under nitrogen at 37 °C. The residues were reconstituted in 150 µL 0.1% formic acid in water:0.1% formic acid in acetonitrile 90:10 (v/v). After centrifugation for 10 min, 15,000g, at room temperature, the supernatants were transferred into autosampler vials with a glass insert. At the same time, to study metabolite glucuronidation, 100 µL urine was mixed with 10 µL 10 mol/L ammonium acetate, pH 5.0, and 100 µL β-glucuronidase (5000 units) in conical glass tubes. Tubes were capped and incubated at 37 °C. After 90 min, 400 µL ice-cold acetonitrile was added to the mixtures, which were then mixed and centrifuged for 10 min, 15,000g, at room temperature. The supernatants were evaporated to dryness under nitrogen at 37 °C. The residues were reconstituted in 150 µL 0.1% formic acid in water:0.1% formic acid in acetonitrile 90:10 (v/v) or 95:5 (v/v) depending on the chromatographic gradient (Section 2.1.7-9). After centrifugation for 10 min, 15,000g, at room temperature, the supernatants were transferred into autosampler vials with a glass insert. The samples were also prepared in the same conditions with 100 µL water instead of β-glucuronidase to ensure that the hydrolysis was enzymatic. Analyses of the incubates and human samples were then performed with a Dionex UltiMate 3000 chromatographic system coupled with a Thermo Scientific

(Waltham, MA, USA) Q Exactive mass spectrometer equipped with a heated electrospray ionization (HESI)-source (LC-HRMS/MS).

2.1.7. Identification of Metabolites using LC-HRMS/MS

Extracted samples were kept in an autosampler at 10 ±1 °C, before injecting 10 µL onto the chromatographic system. LC-HRMS/MS analysis was performed with a Dionex UltiMate 3000 chromatographic system coupled with a Thermo Scientific (Waltham, MA, USA) Q Exactive mass spectrometer equipped with a heated electrospray ionization (HESI) source. Each sample was injected once in positive- and once in negative-ionization mode. LC-HRMS/MS settings were optimized for each compound for a comprehensive metabolite identification.

2.1.8. Instrumental conditions

2.1.8.1. Dipyanone LC-HRMS/MS settings

The separation of compounds was carried out using a Kinetex Biphenyl column (150 × 2.1 mm, 2 µm) from Phenomenex (Torrance, California, USA).

The mobile phases A and B were utilized at a flow rate of 0.4 mL/min under gradient elution conditions: 2% B was held for 2 min, then increased to 25% B over 12 min, followed by a rapid increase to 95% B within 2 min, and held for 4 min. Subsequently, the initial conditions were restored within 0.1 min and maintained for 3.9 min. resulting in a total chromatographic run time of 24 minutes. The column

oven temperature was consistently maintained at 37±1 °C, and the autosampler was kept at 10±1 °C.

All analyses were performed in both positive- and negative-ion modes. The operating parameters included a spray voltage of ±3.5 kV, sheath gas and auxiliary gas flow rates of 50 a.u. and 10 a.u., respectively, a capillary temperature and auxiliary gas heater temperature of 300 °C, and an S-lens radio frequency level of 50 a.u. Notably, no sweep gas flow rate was employed. Prior to each analytical session, mass calibration was performed using certified calibration solutions in both ion modes. To ensure precision, a lock mass list was prepared for positive-ion mode (*m/z* 279.0933, 144.9821, 146.9803) and negative-ion mode (*m/z* 265.1479, 162.9824, 248.9604).

The mass spectrometer acquired from 1 to 20 min of the chromatographic run using full-scan high-resolution mass spectrometry (FullMS) combined with data-dependent MS/MS (ddMS^2). The FullMS parameters were set as follows: *m/z* range of 100 to 650, resolution of 70,000 (FWHM at *m/z* 200), automatic gain control target of 1×10^6, and a maximum injection time of 200 ms. For ddMS^2, the automatic gain control target was 2×10^5, the maximum injection time was 64 ms, the isolation window was *m/z* 1.2, resolution was 17,500, and stepped normalized collision energy values were set at 40, 70, and 90 a.u. Up to five ddMS^2 scans were triggered per FullMS scan, requiring a minimum intensity of 10^4 and a dynamic exclusion of 2.0 seconds. The data-dependent acquisition employed an inclusion list of putative metabolites (Table 1A) derived from *in silico* predictions (Table 1B) and

extrapolated from the metabolism of structural analogues (34,35). Additionally, ions outside the inclusion list could trigger ddMS^2 scans at a lower priority, facilitated by the "pick others if idle" feature. An exclusion list was also created to filter out background noise, identified through blank control sample injections (A:B 95:5 v/v).

Table 1A. Inclusion list used during liquid chromatography-high-resolution tandem mass spectrometry (LC-HRMS/MS) for dipyanone metabolite identification.

Dipyanone			
Transformation	**Elemental composition**	**$[M+H]^+$ *m/z***	**$[M-H]^-$ *m/z***
Parent (Dipyanone)	**$C_{23}H_{29}NO$**	**336.2322**	**334.2176**
+O	$C_{23}H_{29}NO_2$	352.2271	350.2126
+2O	$C_{23}H_{29}NO_3$	368.2220	366.2075
+2H	$C_{23}H_{31}NO$	338.2478	336.2333
-2H+O	$C_{23}H_{27}NO_2$	350.2115	348.1969
+2H+2O	$C_{23}H_{31}NO_3$	370.2377	368.2231
+2H+O	$C_{23}H_{31}NO_2$	354.2428	352.2282
-2H+2O	$C_{23}H_{27}NO_3$	366.2064	364.1918
-2H	$C_{23}H_{27}NO$	334.2165	332.2020
+6C+10H+6O	$C_{29}H_{39}NO_7$	514.2799	512.2654
+6C+8H+7O	$C_{29}H_{37}NO_8$	528.2592	526.2446
+2H+S+3O	$C_{23}H_{31}NO_4S$	418.2047	416.1901
+S+4O	$C_{23}H_{29}NO_5S$	432.1839	430.1694
-4C-6H	$C_{19}H_{23}NO$	282.1852	280.1707
-4C-8H-1O	$C_{19}H_{21}N$	364.1747	262.1601
-1H+2O	$C_{23}H_{28}NO_2+$	350.2115	349.2042

Table 1B. Dipyanone putative metabolites predicted with GLORYx freeware and their prediction score (adjusted score for second-generation metabolites).

Dipyanone

ID	Transformation	Elemental composition	Score	Simplified molecular-input line-entry system (SMILES)
pA1	*N*-Oxidation	$C_{23}H_{29}NO_2$	29%	[O-][N+]3(C(CC(c1ccccc1)(c2ccccc2)C(=O)CC)C)CCCC3
pA2	Pyrrolidine opening to butanal	$C_{23}H_{29}NO_2$	29%	O=C(C(c1ccccc1)(c2ccccc2)CC(NCCCC=O)C)CC
pA3	Oxidation to γ-lactam	$C_{23}H_{27}NO_2$	29%	O=C3N(C(CC(C(=O)CC)(c1ccccc1)c2ccccc2)C)CCC3
pA4	Pyrrolidine hydroxylation (3')	$C_{23}H_{29}NO_2$	29%	O=C(C(c1ccccc1)(c2ccccc2)CC(N3CCC(O)C3)C)CC
pA4-1	+ *O*-Sulfation (hydroxyl)	$C_{23}H_{29}NO_5S$	29%	O=S(=O)(O)OC3CCN(C(CC(C(=O)CC)(c1ccccc1)c2ccccc2)C)C3
pA4-2	+ *O*-Glucuronidation (hydroxyl)	$C_{29}H_{37}NO_8$	28%	O=C(O)C4OC(OC3CN(C(C)CC(c1ccccc1)(c2ccccc2)C(=O)CC)CC3)C(O)C(O)C4O
pA5	Pyrrolidine hydroxylation (2')	$C_{23}H_{29}NO_2$	29%	O=C(C(c1ccccc1)(c2ccccc2)CC(N3CCCC3O)C)CC
pA5-1	+ O-Sulfation (hydroxyl)	$C_{23}H_{29}NO_5S$	28%	O=S(=O)(O)OC3N(C(CC(C(=O)CC)(c1ccccc1)c2ccccc2)C)CCC3

2.1.8.2. Etonitazepipne LC-HRMS/MS setting

Identification of metabolites was conducted using an LC-HRMS/MS system equipped with a Kinetex Biphenyl column (150 × 2.1 mm, 2.6 μm) from Phenomenex (Castel Maggiore, Italy).

Chromatographic separation was achieved with a gradient elution of 0.1% formic acid in water (mobile phase A) and 0.1% formic acid in acetonitrile (mobile phase B) at a flow rate of 0.4 mL/min and a column temperature of 37 °C. The gradient program began with 5% B for 2 minutes, followed by a gradual increase to 25% over 12 minutes, then to 50% over the next 5 minutes, and finally to 95% within 1 minute. The 95% B condition was held for 5 minutes before returning to the initial gradient within 0.1 minutes. The total chromatographic runtime was 30 minutes.

Source settings for the HESI interface were optimized by injecting etonitazepipne at a concentration of 1 μg/mL (A: B 95:5 v/v). The MS parameters included a spray voltage of ±3.5 kV, sheath gas flow rate of 50 a.u., auxiliary gas flow rate of 10 a.u., auxiliary gas and capillary temperatures both set at 300 °C, and an S-lens radio frequency level of 50 a.u. Data acquisition was performed in full-scan HRMS and data-dependent HRMS/MS modes (FullMS/ddMS^2).

The FullMS conditions were as follows: resolution of 70,000 (full width at half maximum at *m/z* 200), mass range of *m/z* 250–720, automatic gain control (AGC) target of 3×10^6, and maximum injection time (IT) of 0.2 seconds. For ddMS^2, the parameters included a resolution of 17,500, topN of 5 (with “pick others if idle” enabled), an intensity threshold of 10^4, a dynamic exclusion window of 2 seconds,

an isolation window of *m/z* 1.2, normalized collision energies of 40, 55, and 80, an AGC target of 2×10^5, and a maximum IT of 0.064 seconds. An inclusion list was created for etonitazepipne (Table 2A). An inclusion list was established based on the *in silico* predictions list made through GloryX freeware(30,31) (Table 2B) and previous publications(36–39). Positive and negative calibration of the orbitrap was performed before the analysis. To increase accuracy, a lock mass list with previously identified background ions was created (40).

Table 2A Inclusion list used during liquid chromatography-high-resolution tandem mass spectrometry (LC-HRMS/MS) for etonitazepipne metabolite identification.

Etonitazepipne

Transformation	Elemental composition	$[M+H]^+$ *m/z*	$[M-H]^-$ *m/z*
-18C-17H-3N-3O	$C_5H_{11}N$	86.0964	84.0819
-16C-15H-3N-2O	$C_7H_{13}NO$	128.107	126.0924
-5C-11H-1N+1O	$C_{18}H_{17}N_3O_4$	340.1292	338.1146
-5C-9H-1N+1O	$C_{18}H_{19}N_3O_4$	342.1448	340.1303
-2C-2H-2O	$C_{21}H_{26}N_4O$	351.2179	349.2034
-5C-11H-1N+2O	$C_{18}H_{17}N_3O_5$	356.1241	354.1095
+4O-6H	$C_{20}H_{22}N_4O_3$	367.1765	365.1619
+2H-2O	$C_{23}H_{30}N_4O$	379.2492	377.2347
-2C-4H	$C_{21}H_{24}N_4O_3$	381.1921	379.1776
-2C-6H+1O	$C_{21}H_{22}N_4O_4$	395.1714	393.1568
-2H-1O	$C_{23}H_{30}N_4O_2$	395.2442	393.2296
-2C-4H+1O	$C_{21}H_{24}N_4O_4$	397.187	395.1725
-1H	$C_{23}H_{27}N_4O_3^+$	407.2078	-
Parent (Etonitazepipne)	**$C_{23}H_{28}N_4O_3$**	**409.2234**	**407.2089**
-5C-9H-N+4O+S	$C_{18}H_{19}N_3O_7S$	422.1016	420.0871
-1H+1O	$C_{23}H_{27}N_4O_4^+$	423.2027	-
-2H+1O	$C_{23}H_{26}N_4O_4$	423.2027	421.1881
+1O	$C_{23}H_{28}N_4O_4$	425.2183	423.2038
+2H+1O	$C_{23}H_{30}N_4O_4$	427.234	425.2194
-2H+2O	$C_{23}H_{26}N_4O_5$	439.1976	437.183
+2O	$C_{23}H_{28}N_4O_5$	441.2132	439.1987
+3O	$C_{23}H_{28}N_4O_6$	457.2082	455.1936
-2C-4H+3O+S	$C_{21}H_{24}N_4O_6S$	461.1489	459.1344
+4O+S	$C_{23}H_{28}N_4O_7S$	505.1751	503.1609
+1C-1H-1N+7O	$C_{24}H_{27}N_3O_{10}$	518.1769	516.1624
+4C+4H+6O	$C_{27}H_{32}N_4O_9$	557.2242	555.2097
+6O+8H+7O	$C_{29}H_{36}N_4O_{10}$	601.2504	599.2359

Table 2B. Etonitazepipne putative metabolites predicted with GLORYx freeware and their prediction score (adjusted score for second-generation metabolites).

Etonitazepipne

ID		Transformation	Elemental composition	Score	Simplified molecular-input line-entry system (SMILES)
m1		Aliphatic hydroxylation	$C_{23}H_{28}N_4O_4$	73%	[O-][N+](=O)c1cc2nc(n(c2cc1)CCN3CCCCC3)Cc4ccc(OC(O)C)cc4
	m1-1	+ Sulfation	$C_{23}H_{28}N_4O_7S$	55%	O=S(=O)(O)OC(Oc1ccc(cc1)Cc2nc4cc([N+]([O-])=O)ccc4n2CCN3CCCCC3)C
	m1-2	+ Hydroxylation (Piperidinyl ring)	$C_{23}H_{28}N_4O_5$	44%	[O-][N+](=O)c1cc2nc(n(c2cc1)CCN3CCCC(O)C3)Cc4ccc(OC(O)C)cc4
	m1-3	+ Hydroxylation (Piperidinyl ring)	$C_{23}H_{28}N_4O_5$	44%	[O-][N+](=O)c1cc2nc(n(c2cc1)CCN3CCCCC3O)Cc4ccc(OC(O)C)cc4
	m1-4	+ Oxidation (Piperidinyl ring)	$C_{23}H_{26}N_4O_5$	44%	[O-][N+](=O)c1cc2nc(n(c2cc1)CCN3C(=O)CCCC3)Cc4ccc(OC(O)C)cc4
	m1-5	+ *N*-oxidation	$C_{23}H_{28}N_4O_5$	44%	[O-][N+](=O)c1cc2nc(n(c2cc1)CC[N+]3([O-])CCCCC3)Cc4ccc(OC(O)C)cc4
	m1-6	+ *N*-dealkylation	$C_{23}H_{28}N_4O_5$	44%	[O-][N+](=O)c1cc2nc(n(c2cc1)CCNCCCCC=O)Cc3ccc(OC(O)C)cc3
	m1-7	+ Hydroxylation	$C_{23}H_{28}N_4O_5$	41%	[O-][N+](=O)c1cc2nc(n(c2cc1)CCN3CCCCC3)Cc4ccc(OC(O)(O)C)cc4
	m1-8	Ketone reduction	$C_{21}H_{24}N_4O_3$	41%	[O-][N+](=O)c1cc2nc(n(c2cc1)CCN3CCCCC3)Cc4ccc(O)cc4
	m1-9	+ Oxidation	$C_{23}H_{26}N_4O_4$	41%	[O-][N+](=O)c1cc2nc(n(c2cc1)CCN3CCCCC3)Cc4ccc(OC(=O)C)cc4
m2		+ *O*-dealkylation	C_2H_6O	73	OCC
	m2-1	+ Sulfation	$C_2H_6O_4S$	70	O=S(=O)(OCC)O
	m2-2	*O*-glucuronidation	$C_8H_{14}O_7$	55	O=C(O)C1OC(OCC)C(O)C(O)C1O
	m2-3	+ Aliphatic hydroxylation	$C_2H_6O_2$	34	OC(O)C
m3		*O*-dealkylation	$C_{21}H_{24}N_4O_3$	73	[O-][N+](=O)c1cc2nc(n(c2cc1)CCN3CCCCC3)Cc4ccc(O)cc4
	m3-1	+ O-glucuronidation	$C_{27}H_{32}N_4O_9$	72	[O-][N+](=O)c1cc2nc(n(c2cc1)CCN3CCCCC3)Cc5ccc(OC4OC(C(=O)O)C(O)C(O)C4O)cc5
	m3-2	+ Sulfation	$C_{21}H_{24}N_4O_6S$	70	O=S(=O)(O)Oc1ccc(cc1)Cc2nc4cc([N+]([O-])=O)ccc4n2CCN3CCCCC3
	m3-3	+ Hydroxylation (Piperidinyl ring)	$C_{21}H_{24}N_4O_4$	40%	[O-][N+](=O)c1cc2nc(n(c2cc1)CCN3CCCCC3O)Cc4ccc(O)cc4
	m3-4	+ Hydroxylation (Piperidinyl ring)	$C_{21}H_{24}N_4O_4$	40%	[O-][N+](=O)c1cc2nc(n(c2cc1)CCN3CCCC(O)C3)Cc4ccc(O)cc4
	m3-5	+ *N*-oxidation	$C_{21}H_{24}N_4O_4$	40%	[O-][N+](=O)c1cc2nc(n(c2cc1)CC[N+]3([O-])CCCCC3)Cc4ccc(O)cc4
	m3-6	+ *N*-dealkylation	$C_{21}H_{24}N_4O_4$	40%	[O-][N+](=O)c1cc2nc(n(c2cc1)CCNCCCCC=O)Cc3ccc(O)cc3
	m3-7	+ Oxidation (N-ethyl piperidinyl ring)	$C_{21}H_{24}N_4O_4$	40%	[O-][N+](=O)c1cc2nc(n(c2cc1)CCN3C(=O)CCCC3)Cc4ccc(O)cc4
	m3-8	Hydroxylation (Phenyl ring)	$C_{21}H_{24}N_4O_4$	30	[O-][N+](=O)c1cc2nc(n(c2cc1)CCN3CCCCC3)Cc4ccc(O)c(O)c4

m4		Oxidation (Piperidinyl ring)	$C_{23}H_{26}N_4O_4$	60	[O-][N+](=O)c1cc2nc(n(c2cc1)CCN3C(=O)CCCC3)Cc4ccc(OCC)cc4
	m4-1	+ Hydroxylation	$C_{23}H_{26}N_4O_5$	44%	[O-][N+](=O)c1cc2nc(n(c2cc1)CCN3C(=O)CCCC3)Cc4ccc(OC(O)C)cc4
	m4-2	+ *O*-dealkylation	$C_{21}H_{22}N_4O_4$	44%	[O-][N+](=O)c1cc2nc(n(c2cc1)CCN3C(=O)CCCC3)Cc4ccc(O)cc4
	m4-3	+ Hydrolysis	$C_{23}H_{28}N_4O_5$	35	[O-][N+](=O)c1cc2nc(n(c2cc1)CCNCCCCC(=O)O)Cc3ccc(OCC)cc3
	m4-4	+ *N*-oxidation	$C_{23}H_{26}N_4O_5$	35	[O-][N+](=O)c1cc2nc(n(c2cc1)CC[N+]3([O-])C(=O)CCCC3)Cc4ccc(OCC)cc4
	m4-5	+ *N*-dealkylation	$C_{23}H_{26}N_4O_5$	35	[O-][N+](=O)c1cc2nc(n(c2cc1)CCNC(=O)CCCC=O)Cc3ccc(OCC)cc3
	m4-6	+ Hydroxylation (Piperidinyl ring)	$C_{23}H_{26}N_4O_5$	35	[O-][N+](=O)c1cc2nc(n(c2cc1)CCN3C(=O)CCCC3O)Cc4ccc(OCC)cc4
	m4-7	+ Oxidation (Piperidinyl ring)	$C_{23}H_{24}N_4O_5$	35	[O-][N+](=O)c1cc2nc(n(c2cc1)CCN3C(=O)CCCC3=O)Cc4ccc(OCC)cc4
	m4-8	+ Hydroxylation (Piperidinyl ring)	$C_{23}H_{26}N_4O_5$	35	[O-][N+](=O)c1cc2nc(n(c2cc1)CCN3C(=O)CCC(O)C3)Cc4ccc(OCC)cc4
	m4-9	+ Hydroxylation (Piperidinyl ring)	$C_{23}H_{26}N_4O_5$	30	[O-][N+](=O)c1cc2nc(n(c2cc1)CCN3C(=O)C(O)CCC3)Cc4ccc(OCC)cc4
m5		Hydroxylation (Piperidinyl ring)	$C_{23}H_{28}N_4O_4$	60	[O-][N+](=O)c1cc2nc(n(c2cc1)CCN3CCCCC3O)Cc4ccc(OCC)cc4
	m5-1	+ Sulfation	$C_{23}H_{28}N_4O_7S$	57	[O-][N+](=O)c1cc2nc(n(c2cc1)CCN3CCCCC3OS(=O)(=O)O)Cc4ccc(OCC)cc4
	m5-2	+ *O*-dealkylation	$C_{21}H_{24}N_4O_4$	44%	[O-][N+](=O)c1cc2nc(n(c2cc1)CCN3CCCCC3O)Cc4ccc(O)cc4
	m5-3	+ Aliphatic hydroxylation	$C_{23}H_{28}N_4O_5$	44%	[O-][N+](=O)c1cc2nc(n(c2cc1)CCN3CCCCC3O)Cc4ccc(OC(O)C)cc4
	m5-4	+ *O*-glucuronidation	$C_{29}H_{36}N_4O_{10}$	36	[O-][N+](=O)c1cc2nc(n(c2cc1)CCN4C(OC3OC(C(=O)O)C(O)C(O)C3O)CCCC4)Cc5ccc(OCC)cc5
	m5-5	+ *N*-dealkylation	$C_{23}H_{28}N_4O_5$	26	[O-][N+](=O)c1cc2nc(n(c2cc1)CCNCCCCC(=O)O)Cc3ccc(OCC)cc3
	m5-6	+ Oxidation (Piperidinyl ring)	$C_{23}H_{26}N_4O_4$	26	[O-][N+](=O)c1cc2nc(n(c2cc1)CCN3C(=O)CCCC3)Cc4ccc(OCC)cc4
	m5-7	*N*-oxidation	$C_{23}H_{28}N_4O_5$	26	[O-][N+](=O)c1cc2nc(n(c2cc1)CC[N+]3([O-])CCCCC3O)Cc4ccc(OCC)cc4
	m5-8	Aliphatic hydroxylation	$C_{23}H_{28}N_4O_5$	26	[O-][N+](=O)c1cc2nc(n(c2cc1)CCN3CCCC(O)C3O)Cc4ccc(OCC)cc4
	m5-9	Hydrolysis	$C_{23}H_{28}N_4O_4$	26	[O-][N+](=O)c1cc2nc(n(c2cc1)CCNCCCCC=O)Cc3ccc(OCC)cc3
	m5-10	+ Aliphatic Hydroxylation	$C_{23}H_{28}N_4O_5$	26	[O-][N+](=O)c1cc2nc(n(c2cc1)CCN3CCCCC3(O)O)Cc4ccc(OCC)cc4
m6		+ Hydroxylation (Piperidinyl ring)	$C_{23}H_{28}N_4O_4$	60	[O-][N+](=O)c1cc2nc(n(c2cc1)CCN3CCCC(O)C3)Cc4ccc(OCC)cc4
	m6-1	+ Sulfation	$C_{23}H_{28}N_4O_7S$	58	[O-][N+](=O)c1cc2nc(n(c2cc1)CCN3CCCC(OS(=O)(=O)O)C3)Cc4ccc(OCC)cc4
	m6-2	+*O*-glucuronidation	$C_{29}H_{36}N_4O_{10}$	52	[O-][N+](=O)c1cc2nc(n(c2cc1)CCN4CC(OC3OC(C(=O)O)C(O)C(O)C3O)CCC4)Cc5ccc(OCC)cc5
	m6-3	+ O-dealkylation	$C_{21}H_{24}N_4O_4$	44%	[O-][N+](=O)c1cc2nc(n(c2cc1)CCN3CCCC(O)C3)Cc4ccc(O)cc4
	m6-4	+ Aliphatic hydroxylation	$C_{23}H_{28}N_4O_5$	44%	[O-][N+](=O)c1cc2nc(n(c2cc1)CCN3CCCC(O)C3)Cc4ccc(OC(O)C)cc4
m7		+ *N*-oxidation	$C_{23}H_{28}N_4O_4$	60	[O-][N+](=O)c1cc2nc(n(c2cc1)CC[N+]3([O-])CCCCC3)Cc4ccc(OCC)cc4
	m7-1	+ *O*-dealkylation	$C_{21}H_{24}N_4O_4$	44%	[O-][N+](=O)c1cc2nc(n(c2cc1)CC[N+]3([O-])CCCCC3)Cc4ccc(O)cc4
	m7-2	+ Aliphatic Hydroxylation	$C_{23}H_{28}N_4O_5$	44%	[O-][N+](=O)c1cc2nc(n(c2cc1)CC[N+]3([O-])CCCCC3)Cc4ccc(OC(O)C)cc4

m8		+ *N*-dealkylation	$C_{23}H_{28}N_4O_4$	60	[O-][N+](=O)c1cc2nc(n(c2cc1)CCNCCCCC=O)Cc3ccc(OCC)cc3
	m8-1	+ Aliphatic hydroxylation	$C_{23}H_{28}N_4O_5$	38	[O-][N+](=O)c1cc2nc(n(c2cc1)CCNCCCCC=O)Cc3ccc(OC(O)C)cc3
	m8-2	+ *O*-dealkylation	$C_{21}H_{24}N_4O_4$	38	[O-][N+](=O)c1cc2nc(n(c2cc1)CCNCCCCC=O)Cc3ccc(O)cc3
	m8-3	+ Aldehyde reduction	$C_{23}H_{30}N_4O_4$	25%	[O-][N+](=O)c1cc2nc(n(c2cc1)CCNCCCCCO)Cc3ccc(OCC)cc3
	m8-4	+ Aldehyde Oxidation	$C_{23}H_{28}N_4O_5$	25%	[O-][N+](=O)c1cc2nc(n(c2cc1)CCNCCCCC(=O)O)Cc3ccc(OCC)cc3

2.1.8.3. Protonitazepyne and Metonitazepyne LC-HRMS/MS setting

Analytes were separated using a Kinetex Biphenyl column (150 × 2.1 mm, 2 μm) from Phenomenex (Torrance, CA, USA) with a flow rate was of 0.4 mL/min.

The gradient elution of 0.1% formic acid in water (mobile phase A) and 0.1% formic acid in acetonitrile (mobile phase B) was set as follow: 5% B held for 2 min, increased to 25% B within 14 min, increased to 50% within 19 min, increased to 95% in 1 min, and held for 5 min; initial conditions were restored within 0.1 min and maintained for 4.9 min. The chromatographic run lasted 30 min. The column oven was set at 37 ± 1 °C, and the autosampler temperature was 10 ± 1 °C. Analyses were carried out in both positive- and negative-ion modes through separate injections, using the following HESI source parameters: spray voltage, ± 3.5 kV; sheath gas and auxiliary flow rates, 50 a.u. and 10 a.u., respectively; capillary temperature and auxiliary gas heater temperature, 300 °C; S-lens radio frequency level, 50 a.u.; sweep gas flow rate was not used. Mass calibration was performed with certified calibration solutions prior to the analytical session, both in positive and negative ion modes. To enhance accuracy, a lock mass list was utilized in positive-ion mode, targeting specific ions (*m/z* 279.1590, 282.27914, 284.29479). Mass spectrometer data was acquired from 1 to 25 min of the chromatographic run in full-scan HRMS (FullMS)/data-dependent MS/MS (ddMS^2) mode. FullMS settings were: range, *m/z* 200 to 750; resolution at full width at half maximum at *m/z* 200, 70,000; automatic gain control (AGC) target, 3×10^6; and maximum injection time (IT), 200 ms. ddMS^2 settings were: ACG target, 2×10^5; maximum

IT, 64 ms; isolation window, *m/z* 1.2; resolution, 17,500; and stepped normalised collision energy (NCE), 40, 55, and 80 a.u. A maximum number of five ddMS^2 scans were triggered for each FullMS scan (minimum intensity, 10^4; dynamic exclusion, 2.0 s). An inclusion list of putative metabolites was created for each analyte (Tables 3A, 4A), based on *in silico* predictions (Tables 3B, 4B) and previous postulation (15,29,36–38,41–43). Although ions outside the inclusion list could trigger ddMS^2 scans, they were given lower priority via the "pick others if idle" option. Additionally, an exclusion list was compiled for both analytes to filter out background noise, determined by blank control sample injections (A: B 95:5 v/v).

Table 3A. Inclusion list used during liquid chromatography-high-resolution tandem mass spectrometry (LC-HRMS/MS) for protonitazepyne metabolite identification.

Protonitazepyne			
Transformation	**Elemental composition**	**$[M+H]^+$ *m/z***	**$[M-H]^-$ *m/z***
Parent	**$C_{23}H_{28}N_4O_3$**	**409.2234**	**407.2089**
-3C-6H	$C_{20}H_{22}N_4O_3$	367.1765	365.1619
+3C+2H+6O	$C_{26}H_{30}N_4O_9$	543.2086	541.1940
+O	$C_{23}H_{28}N_4O_4$	425.2183	423.2038
-2H+O	$C_{23}H_{26}N_4O_4$	423.2027	421.1881
+2H+O	$C_{23}H_{30}N_4O_4$	427.2340	425.2194
+2O	$C_{23}H_{28}N_4O_5$	441.2132	439.1987
+2H-2O	$C_{23}H_{30}N_4O$	379.2492	377.2347
-3C-6H+O	$C_{20}H_{22}N_4O_4$	383.1714	381.1568
-3C-8H+O	$C_{20}H_{20}N_4O_4$	381.1557	379.1412
+6C-8H+7O	$C_{29}H_{36}N_4O_{10}$	601.2504	599.2359
-3C-4H+O	$C_{20}H_{24}N_4O_4$	385.1870	383.1725
-3C-6H+2O	$C_{20}H_{22}N_4O_5$	399.1663	397.1517
-2H+2O	$C_{23}H_{26}N_4O_5$	439.1976	437.1830
-4C-7H-N+O	$C_{19}H_{21}N_3O_4$	356.1605	354.1459
-4C-6H	$C_{19}H_{22}N_4O_3$	355.1765	353.1619
+3C+2H+7O	$C_{26}H_{30}N_4O_{10}$	559.2035	557.1889
+2H+2O	$C_{23}H_{30}N_4O_5$	443.2289	441.2143
+3O	$C_{23}H_{28}N_4O_6$	457.2082	455.1936
+6C+10H+7O	$C_{29}H_{38}N_4O_{10}$	603.2661	601.2515
+6C+8H+8O	$C_{29}H_{36}N_4O_{11}$	617.2453	615.2308
-3C-4H-2O	$C_{20}H_{24}N_4O$	337.2023	335.1877
+2C+4H-O	$C_{25}H_{32}N_4O_2$	421.2598	419.2453
-7C-13H-N+O	$C_{16}H_{15}N_3O_4$	314.1135	312.0990
+2C+H-N+7O	$C_{25}H_{29}N_3O_{10}$	532.1926	530.1780
-4C-7H-N+2O	$C_{19}H_{21}N_3O_5$	372.1554	370.1408
-7C-12H	$C_{16}H_{16}N_4O_3$	313.1295	311.1150
-O	$C_{23}H_{28}N_4O_2$	393.2285	391.2140
-3C-6H-O	$C_{20}H22N_4O_2$	351.1816	349.1670
+2H-O	$C_{23}H_{30}N_4O_2$	395.2442	393.2296
-3C-4H-O	$C_{20}H_{24}N_4O_2$	353.1972	351.1827
-3C-6H+3O+S	$C_{20}H_{22}N_4O_6S$	447.1333	445.1187
+4O+S	$C_{23}H_{28}N_4O_7S$	505.1751	503.1606
-4C-7H-N+4O+S	$C_{19}H_{21}N_3O_7S$	436.1173	434.1027

Table 4A. Inclusion list used during liquid chromatography-high-resolution tandem mass spectrometry (LC-HRMS/MS) for metonitazepyne metabolite identification.

Metonitazepyne			
Transformation	**Elemental composition**	**$[M+H]^+$ *m/z***	**$[M-H]^-$ *m/z***
Parent	**$C_{21}H_{24}N_4O_3$**	**381.1921**	**379.1776**
-C-2H	$C_{20}H_{22}N_4O_3$	367.1765	365.1619
+5C+6H+6O	$C_{26}H_{30}N_4O_9$	543.2086	541.1940
+O	$C_{21}H_{24}N_4O_4$	397.1870	395.1725
-2H+O	$C_{21}H_{22}N_4O_4$	395.1714	393.1568
+2H+O	$C_{21}H_{26}N_4O_4$	399.2027	397.1881
+2O	$C_{21}H_{24}N_4O_5$	413.1819	411.1674
+2H-2O	$C_{21}H_{26}N_4O$	351.2179	349.2034
-C-2H+O	$C_{20}H_{22}N_4O_4$	383.1714	381.1568
-C-4H+O	$C_{20}H_{20}N_4O_4$	381.1557	379.1412
+6C-8H+7O	$C_{27}H_{32}N_4O_{10}$	573.2191	571.2046
-C+O	$C_{20}H_{24}N_4O_4$	385.1870	383.1725
-C-2H+2O	$C_{20}H_{22}N_4O_5$	399.1663	397.1517
-2H+2O	$C_{21}H_{22}N_4O_5$	411.1663	409.1517
-4C-7H-N+O	$C_{17}H_{17}N_3O_4$	328.1292	326.1146
-4C-6H	$C_{17}H_{18}N_4O_3$	327.1452	325.1306
+5C+6H+7O	$C_{26}H_{30}N_4O_{10}$	559.2035	557.1889
+2H+2O	$C_{21}H_{26}N_4O_5$	415.1976	413.1830
+3O	$C_{21}H_{24}N_4O_6$	429.1769	427.1623
+6C+10H+7O	$C_{27}H_{34}N_4O_{10}$	575.2348	573.2202
+6C+8H+8O	$C_{27}H_{32}N_4O_{11}$	589.2140	587.1995
-C-2O	$C_{20}H_{24}N_4O$	337.2023	335.1877
+2C+4H-O	$C_{23}H_{28}N_4O_2$	393.2285	391.2140
-5C-9H-N+O	$C_{16}H_{15}N_3O_4$	314.1135	312.0990
+2C+H-N+7O	$C_{23}H_{25}N_3O_{10}$	504.1613	502.1467
-4C-7H-N+2O	$C_{17}H_{17}N_3O_5$	344.1241	342.1095
-5C-8H	$C_{16}H_{16}N_4O_3$	313.1295	311.1150
-O	$C_{21}H_{24}N_4O_2$	365.1972	363.1827
-C-2H-O	$C_{20}H_{22}N_4O_2$	351.1816	349.1670
+2H-O	$C_{21}H_{26}N_4O_2$	367.2129	365.1983
-C-O	$C_{20}H_{24}N_4O_2$	353.1972	351.1827
-C-2H+3O+S	$C_{20}H_{22}N_4O_6S$	447.1333	445.1187
+4O+S	$C_{21}H_{24}N_4O_7S$	477.1438	475.1293
-4C-7H-N+4O+S	$C_{17}H_{17}N_3O_7S$	408.0860	406.0714

Table 3B. Protonitazepyne putative metabolites predicted with GLORYx freeware and their prediction score (adjusted score for second-generation metabolites)

Protonitazepyne					
ID		**Transformation**	**Elemental composition**	**Score**	**Simplified molecular-input line-entry system (SMILES)**
pB1		Carboxylation	$C_{23}H_{26}N_4O_5$	62%	O=C(O)CCOc1ccc(cc1)Cc2nc4cc([N+]([O-])=O)ccc4n2CCN3CCCC3
	pB1-1	+*O*-glucuronidation	$C_{29}H_{34}N_4O_{11}$	42%	O=C(OC1OC(C(=O)O)C(O)C(O)C1O)CCOc2ccc(cc2)Cc4nc3cc([N+]([O-])=O)ccc3n4CCN5CCCC5
pB2		Hydroxylation	$C_{23}H_{28}N_4O_4$	62%	[O-][N+](=O)c1cc2nc(n(c2cc1)CCN3CCCC3)Cc4ccc(OCCCO)cc4
	pB2-1	+ Sulfation	$C_{23}H_{28}N_4O_7S$	44%	O=S(=O)(O)OCCCOc1ccc(cc1)Cc2nc4cc([N+]([O-])=O)ccc4n2CCN3CCCC3
	pB2-2	+ *O*-glucuronidation	$C_{29}H_{36}N_4O_{10}$	33%	[O-][N+](=O)c1cc2nc(n(c2cc1)CCN3CCCC3)Cc5ccc(OCCCOC4OC(C(=O)O)C(O)C(O)C4O)cc5
pB3		Hydroxylation	$C_{23}H_{28}N_4O_4$	62%	[O-][N+](=O)c1cc2nc(n(c2cc1)CCN3CCCC3)Cc4ccc(OCC(O)C)cc4
	pB3-1	+ Sulfation	$C_{23}H_{28}N_4O_7S$	59%	O=S(=O)(O)OC(C)COc1ccc(cc1)Cc2nc4cc([N+]([O-])=O)ccc4n2CCN3CCCC3
	pB3-2	+ *O*-glucuronidation	$C_{29}H_{36}N4O_{10}$	49%	[O-][N+](=O)c1cc2nc(n(c2cc1)CCN3CCCC3)Cc5ccc(OCC(OC4OC(C(=O)O)C(O)C(O)C4O)C)cc5
	pB3-3	+ Hydroxylation	$C_{23}H_{28}N_4O_5$	25%	[O-][N+](=O)c1cc2nc(n(c2cc1)CCN3CCCC3)Cc4ccc(OCC(O)(O)C)cc4
	pB3-4	+ Oxidation	$C_{23}H_{26}N_4O_4$	25%	[O-][N+](=O)c1cc2nc(n(c2cc1)CCN3CCCC3)Cc4ccc(OCC(=O)C)cc4
pB4		*O*-dealkylation	C_3H_8O	62%	OCCC
	pB4-1	+ Sulfation	$C_3H_8O_4S$	55%	O=S(=O)(OCCC)O
	pB4-2	+ *O*-glucuronidation	$C_9H_{16}O_7$	44%	O=C(O)C1OC(OCCC)C(O)C(O)C1O
	pB4-3	+ Oxidation	$C_3H_6O_2$	33%	O=C(O)CC
	pB4-4	+ Oxidation	$C_3H_8O_2$	33%	O=CCC
	pB4-5	+ Hydroxylation	$C_3H_8O_2$	30%	OCCCO
	pB4-6	+ Hydroxylation	$C_3H_8O_2$	30%	OCC(O)C

	pB4-7	+ Hydroxylation	$C_3H_8O_2$	30%	OC(O)CC
	pB4-8	+ Carboxylation	$C_3H_6O_3$	30%	O=C(O)CCO
pB5		*O*-dealkylation	$C_{20}H_{22}N_4O_3$	62%	[O-][N+](=O)c1cc2nc(n(c2cc1)CCN3CCCC3)Cc4ccc(O)cc4
	pB5-1	+ *O*-glucuronidation	$C_{26}H_{30}N_4O_9$	61%	[O-][N+](=O)c1cc2nc(n(c2cc1)CCN3CCCC3)Cc5ccc(OC4OC(C(=O)O)C(O)C(O)C4O)cc5
	pB5-2	+ Sulfation	$C_{20}H_{22}N_4O_6S$	59%	O=S(=O)(O)Oc1ccc(cc1)Cc2nc4cc([N+]([O-])=O)ccc4n2CCN3CCCC3
	pB5-3	+ Oxidation	$C_{20}H_{22}N_4O_4$	29%	[O-][N+](=O)c1cc2nc(n(c2cc1)CCN3CCCC3)Cc4ccc(O)c(O)c4
pB6		Hydroxylation	$C_{23}H_{28}N_4O_4$	62%	[O-][N+](=O)c1cc2nc(n(c2cc1)CCN3CCCC3)Cc4ccc(OC(O)CC)cc4
	pB6-1	+ Sulfation	$C_{23}H_{28}N_4O_7S$	45%	O=S(=O)(O)OC(Oc1ccc(cc1)Cc2nc4cc([N+]([O-])=O)ccc4n2CCN3CCCC3)CC
	pB6-2	+ Oxidation	$C_3H_6O_2$	35%	O=C(O)CC
	pB6-3	+ Oxidation	$C_{20}H_{22}N_4O_3$	35%	[O-][N+](=O)c1cc2nc(n(c2cc1)CCN3CCCC3)Cc4ccc(O)cc4
	pB6-4	+ Oxidation	$C_{23}H_{28}N_4O_5$	35%	[O-][N+](=O)c1cc2nc(n(c2cc1)CCN3CCCC3)Cc4ccc(OC(O)C(O)C)cc4
	pB6-5	+ Oxidation	$C_{23}H_{28}N_4O_5$	35%	[O-][N+](=O)c1cc2nc(n(c2cc1)CCN3CCCC3)Cc4ccc(OC(O)CCO)cc4
	pB6-6	+ Carboxylation	$C_{23}H_{26}N_4O_6$	35%	O=C(O)CC(O)Oc1ccc(cc1)Cc2nc4cc([N+]([O-])=O)ccc4n2CCN3CCCC3
	pB6-7	+ Oxidation	$C_{23}H_{26}N_4O_4$	35%	[O-][N+](=O)c1cc2nc(n(c2cc1)CCN3CCCC3)Cc4ccc(OC(=O)CC)cc4
	pB6-8	+ Hydroxylation	$C_{23}H_{28}N_4O_5$	35%	[O-][N+](=O)c1cc2nc(n(c2cc1)CCN3CCCC3)Cc4ccc(OC(O)(O)CC)cc4
pB7		Oxidative Cleavage	C_3H_6O	62%	O=CCC
	pB7-1	+ Aliphatic reduction	C_3H_8O	31%	OCCC
	pB7-2	+ Dehydrogenation	C_3H_4O	31%	O=C\C=C
	pB7-3	+ Oxidation	$C_3H_6O_2$	31%	O=C(O)CC
	pB7-4	+ Carboxylation	$C_3H_4O_3$	31%	O=CCC(=O)O
	pB7-5	+ Hydroxylation	$C_3H_6O_2$	31%	O=CCCO
	pB7-6	+ Hydroxylation	$C_3H_6O_2$	31%	O=CC(O)C
pB8		*N*-dealkylation	$C_{23}H_{28}N_4O_4$	33%	[O-][N+](=O)c1cc2nc(n(c2cc1)CCNCCCC=O)Cc3ccc(OCCC)cc3
pB9		*N*-oxidation	$C_{23}H_{28}N_4O_4$	33%	[O-][N+](=O)c1cc2nc(n(c2cc1)CC[N+]3([O-])CCCC3)Cc4ccc(OCCC)cc4

pB91	+ Sulfation	$C_{23}H_{28}N_4O_7S$	31%	[O-][N+](=O)c1cc2nc(n(c2cc1)CCN3CCCC3OS(=O)(=O)O)Cc4ccc(OCCC)cc4
pB10	Hydroxylation	$C_{23}H_{28}N_4O_4$	33%	[O-][N+](=O)c1cc2nc(n(c2cc1)CCN3CCCC3O)Cc4ccc(OCCC)cc4
pB10-1	+ Sulfation	$C_{23}H_{28}N_4O_7S$	32%	[O-][N+](=O)c1cc2nc(n(c2cc1)CCN3CCC(OS(=O)(=O)O)C3)Cc4ccc(OCCC)cc4
pB10-2	+ *O*-glucuronidation	$C_{29}H_{36}N_4O_{10}$	26%	[O-][N+](=O)c1cc2nc(n(c2cc1)CCN4CC(OC3OC(C(=O)O)C(O)C(O)C3O)CC4)Cc5ccc(OCCC)cc5
pB11	Hydroxylation	$C_{23}H_{28}N_4O_4$	33%	[O-][N+](=O)c1cc2nc(n(c2cc1)CCN3CCC(O)C3)Cc4ccc(OCCC)cc4
pB12	Oxidation	$C_{23}H_{26}N_4O_4$	33%	[O-][N+](=O)c1cc2nc(n(c2cc1)CCN3C(=O)CCC3)Cc4ccc(OCCC)cc4

Table 4B. Metonitazepyne putative metabolites predicted with GLORYx freeware and their prediction score (adjusted score for second-generation metabolites)

Metonitazepyne					
ID		**Transformation**	**Elemental composition**	**Score**	**Simplified molecular-input line-entry system (SMILES)**
pA1		Hydroxylation	$C_{21}H_{24}N_4O_4$	64%	[O-][N+](=O)c1cc2nc(n(c2cc1)CCN3CCCC3)Cc4ccc(OCO)cc4
	pA1-1	+ Sulfation	$C_{21}H_{24}N_4O_7S$	49%	O=S(=O)(O)OCOc1ccc(cc1)Cc2nc4cc([N+]([O-])=O)ccc4n2CCN3CCCC3
	pA1-2	+ Hydroxylation	$C_{21}H_{24}N_4O_5$	37%	[O-][N+](=O)c1cc2nc(n(c2cc1)CCN3CCCC3)Cc4ccc(OC(O)O)cc4
	pA1-3	+ Oxidation	$C_{21}H_{22}N_4O_4$	37%	[O-][N+](=O)c1cc2nc(n(c2cc1)CCN3CCCC3)Cc4ccc(OC=O)cc4
	pA1-4	+ Oxidation	CH_2O_2	37%	O=CO
	pA1-5	Oxidation	$C_{20}H_{22}N_4O_3$	37%	[O-][N+](=O)c1cc2nc(n(c2cc1)CCN3CCCC3)Cc4ccc(O)cc4
pA2		*O*-demethylation	$C_{20}H_{22}N_4O_3$	64%	[O-][N+](=O)c1cc2nc(n(c2cc1)CCN3CCCC3)Cc4ccc(O)cc4
	pA2-1	+ O-glucuronidation	$C_{26}H_{30}N_4O_9$	63%	[O-][N+](=O)c1cc2nc(n(c2cc1)CCN3CCCC3)Cc5ccc(OC4OC(C(=O)O)C(O)C(O)C4O)cc5
	pA2-2	+ Sulfation	$C_{20}H_{22}N_4O_6S$	61%	O=S(=O)(O)Oc1ccc(cc1)Cc2nc4cc([N+]([O-])=O)ccc4n2CCN3CCCC3
	pA2-3	+ Hydroxylation	$C_{20}H_{22}N_4O_4$	30%	[O-][N+](=O)c1cc2nc(n(c2cc1)CCN3CCCC3)Cc4ccc(O)c(O)c4
pA3		Hydroxylation	$C_{21}H_{24}N_4O_4$	33%	[O-][N+](=O)c1cc2nc(n(c2cc1)CCN3CCCC3O)Cc4ccc(OC)cc4
	pA3-1	+ Sulfation	$C_{21}H_{24}N_4O_7S$	32%	[O-][N+](=O)c1cc2nc(n(c2cc1)CCN3CCCC3OS(=O)(=O)O)Cc4ccc(OC)cc4
pA4		*N*-dealkylation	$C_{21}H_{24}N_4O_4$	33%	[O-][N+](=O)c1cc2nc(n(c2cc1)CCNCCCC=O)Cc3ccc(OC)cc3
pA5		*N*-oxidation	$C_{21}H_{24}N_4O_4$	33%	[O-][N+](=O)c1cc2nc(n(c2cc1)CC[N+]3([O-])CCCC3)Cc4ccc(OC)cc4
pA6		Hydroxylation	$C_{21}H_{24}N_4O_4$	33%	[O-][N+](=O)c1cc2nc(n(c2cc1)CCN3CCC(O)C3)Cc4ccc(OC)cc4
	pA6-1	+ Sulfation	$C_{21}H_{24}N_4O_7S$	32%	[O-][N+](=O)c1cc2nc(n(c2cc1)CCN3CCC(OS(=O)(=O)O)C3)Cc4ccc(OC)cc4
	pA6-2	+ O-glucuronidation	$C_{27}H_{32}N_4O_{10}$	27%	[O-][N+](=O)c1cc2nc(n(c2cc1)CCN4CC(OC3OC(C(=O)O)C(O)C(O)C3O)CC4)Cc5ccc(OC)cc5
pA7		Oxidation	$C_{21}H_{22}N_4O_4$	33%	[O-][N+](=O)c1cc2nc(n(c2cc1)CCN3C(=O)CCC3)Cc4ccc(OC)cc4

2.1.9. Data mining

LC-HRMS/MS data analysis was performed with Thermo Fisher Scientific software Compound Discover (CD) (version 3.2.0.421), applying a workflow previously developed with minor modifications to suit molecules and the optimized LC-HRMS/MS conditions (29). The LC-HRMS/MS raw data from incubates and controls were screened with a dual targeted/untargeted approach as follows: 1) relevant spectra were extracted; 2) retention times were aligned between samples to allow comparison; 3a) the ions were compared to a list of theoretical metabolites generated according to *in silico* predictions and postulation (intensity threshold, 5×10^3; HRMS mass tolerance, 5 ppm) then matches were compared to mzCloud (Drugs of Abuse/Illegal Drugs database), ChemSpider (Cayman Chemical, DrugBank), and HighResNPS online databases (HRMS mass tolerance, 5 ppm; HRMS/MS mass tolerance; 10 ppm); 3b) the HRMS/MS spectra and theoretical elemental composition of the ions were compared to mzCloud, ChemSpider, and HighResNPS online databases (intensity threshold, 10^5; HRMS mass tolerance, 5 ppm; HRMS/MS mass tolerance; 10 ppm); and 4) the results from 3a) and 3b) were merged and manually finally screened by the operator for final identification and structural elucidation (Fig. 7).

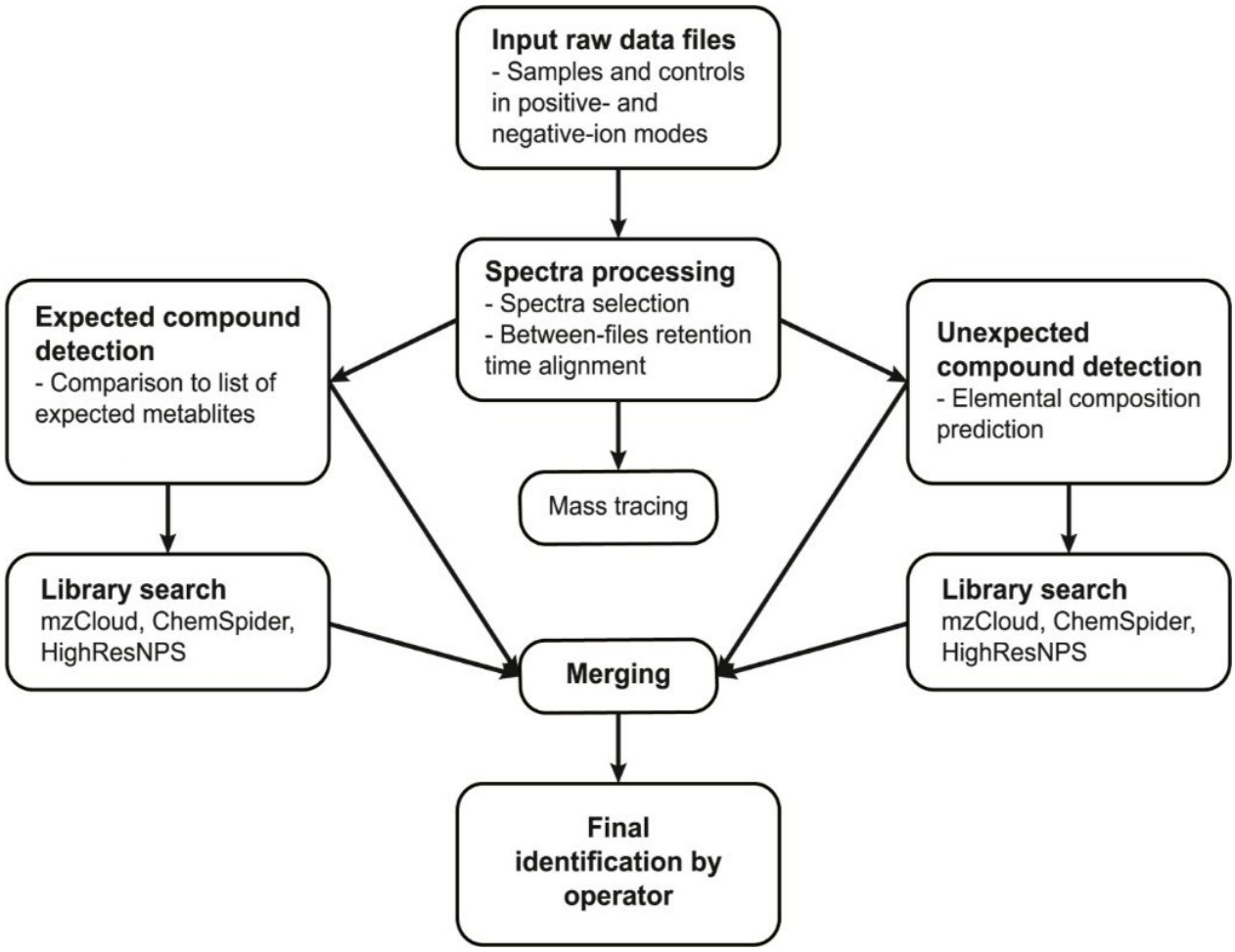


Figure 7: Compound Discoverer Workflow

3. μ-, κ-, and δ- Opioid receptor pharmacological characterization

3.1. Materials and methods

3.1.1. Chemicals and reagents

Human MOR, DOR, and KOR membrane and the GTP Gi Binding assay kit were purchased from Revvity (Milan, Italy). The kit included the following components: GTP Eu Cryptate reagent, GTP d2 antibody, GDP, $MgCl_2$, GTPγS, Gi protein control, and Stimulation Buffer.

3.1.2. Instrumental conditions

The fluorescence resonance energy transfer (FRET) signal was measured using a Multilabel Plate reader (PerkinlElmer), Fluorescence intensity ratios at 665 nm and 620 nm were calculated to mitigate photophysical interference (delay: 100 μs; total measurement window: 200 μs).

The data were normalized to the maximal response observed with the corresponding reference receptor agonist, which was set to 100%. Concentration-response relationships were analyzed using GraphPad Prism software (v10.4.0) to determine EC_{50} values (potency) and E_{max} (efficacy).

3.1.2.1. HTRF-based GTP Gi binding assay

The activation of MOR, KOR, and DOR receptors was assessed through a HTRF®-based GTP Gi binding assay. In this method (44,45), a test compound was incubated with a membrane preparation containing recombinant or native GPCRs (MOR, KOR, or DOR). GPCR activation via agonist binding initiated the exchange of GDP for a non-hydrolyzable GTP analogue conjugated to a europium cryptate donor (Eu-GTP). The proximity of a d2-labeled anti-Gαi monoclonal antibody acceptor to the donor produced a measurable FRET signal, proportional to Gαi activation (25,27).

The assay was conducted in a total volume of 20 μL, comprising a stimulation buffer supplemented with optimized GDP and $MgCl_2$ concentrations, the test compound (dipyanone) or a reference agonist (MOR: fentanyl, KOR: U-50488, DOR: SNC-80), a detection mix containing equal volumes of europium cryptate and d2-labeled

antibody, and the MOR, KOR, or DOR membrane preparation. Non-specific binding was evaluated by introducing 25 µmol/L GTPγS to saturate binding sites and establish background fluorescence levels.

A positive control using a recombinant Gαi subunit was included to validate detection reagents, as both the Eu-GTP analogue and d2-antibody bind to this subunit. Membranes were incubated at room temperature overnight. Dipyanone and reference agonists were prepared in a 90:10 mixture of dimethyl sulfoxide and supplemented stimulation buffer, with final concentrations ranging from 10^{-5} to 10^{-11} mol/L. Each concentration was tested in duplicate, and all experiments were performed in triplicate (n=3).

FRET signals were recorded using the Multilabel Plate Reader, calculating fluorescence ratios at 665/620 nm to minimize photophysical interference (delay: 100 µs; measurement window: 200 µs). Data were normalized to the maximal signal of the respective reference agonist and analyzed for EC_{50} and Emax values using GraphPad Prism (v. 10.2.3).

3.1.3. Data analysis and statistical methods

Raw data were processed using Excel 365 Version 2107 for Windows. For analysis of the raw data, the percentage of the measured signal above the basal activity was determined. Outlier testing was performed using Dixon test (α=0.05). All measured values were normalized to the E_{max} (top value of best fit values) of the reference compound for MOR, DOR, and KOR.

Concentration-response curves were analysed using GraphPad Prism 10 (Version 10.4.0; GraphPad Software Inc., La Jolla, CA, USA). Nonlinear regression (three-parameter model with Hill slope fixed at 1) was applied to fit the curves and determine EC_{50} values (potency) with 95% confidence intervals, as well as Emax values (efficacy) relative to the Emax of the reference compound, also reported with 95% confidence intervals.

4. Results

4.1. Metabolites identification in human hepatocyte & pHLM

4.1.1. Etonitazepipne metabolites identification in pHLM

After 2 h incubation with pHLM a total of 19 metabolites were detected. *In vivo* authentic urine sample analysis, with and without enzymatic hydrolysis led to the detection of 13 and 12 metabolites, respectively. A total of 23 metabolites were found overall, after combining the results from the pHLM incubation and the authentic urine sample. The most pronounced transformations were hydroxylation, O-dealkylation, oxidation, and combinations thereof. A1–A23 metabolic transformation $[M+H]^+$ accurate mass, A1–A23 metabolic transformation $[M+H]^+$ accurate mass, elemental composition, retention time, Δ ppm, chromatographic peak areas are reported in Table 3 (33).

In vivo etonitazepipne metabolic fate is suggested in Figure 2. Extracted-ion chromatogram of etonitazepipne and metabolites in positive ionization mode of pHLM (A), hydrolyzed urine sample (B), non-hydrolyzed urine sample (C) is

shown in Figure 8A–C. Extracted-ion chromatograms of etonitazepipne and its metabolites are presented in positive ionization mode for the pHLM (A), hydrolyzed urine sample (B), and non-hydrolyzed urine sample (C), shown in Figure 7A–C. Table 5 lists the metabolic transformations, retention time, accurate mass, delta ppm error, elemental composition, and chromatographic peak areas for both the pHLM and urine samples after the 2-hour incubation with pHLM. The proposed *in vivo* metabolic pathway of etonitazepipne is depicted in Figure 9 (33).

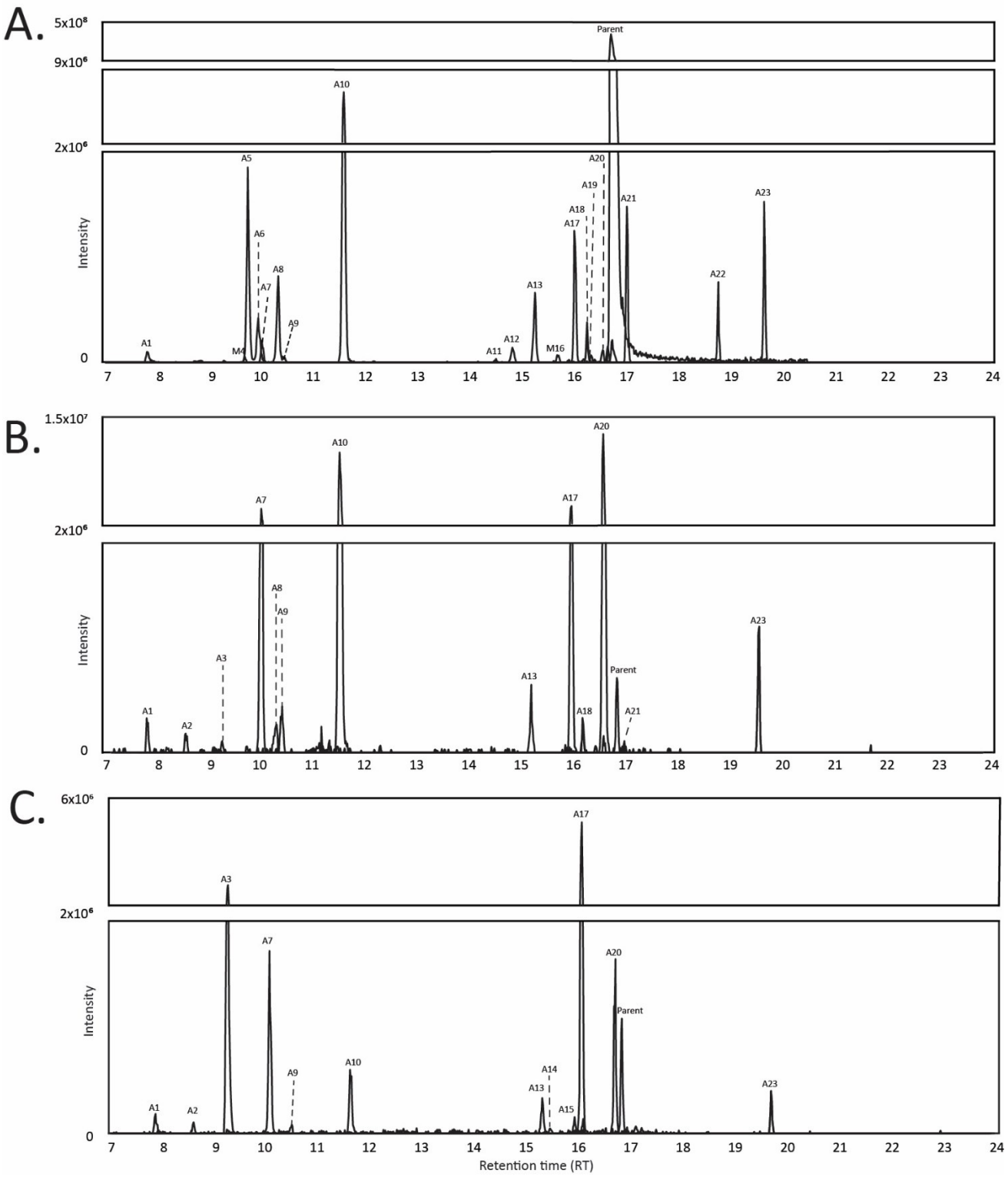


Figure 8: Extracted-ion chromatogram of etonitazepipne and metabolites in positive ionization mode of pHLM (A), hydrolyzed urine sample (B), non-hydrolyzed urine sample (C). Mass tolerance, 5 ppm.

Table 5: Metabolic transformation, retention time, accurate mass of molecular ion hydrogen adduct in positive-ion mode, delta ppm error, elemental composition, chromatographic peak area of pHLM and urine sample of etonitazepipne and metabolites after 2-h incubation with pHLM. -, not applicable. *,.

ID	Biotransformation	RT, min	*m/z* [M+H]+ [M-H]-	Mass error, (Δppm)	Elemental composition	Peak area in incubates: $[M+H]^+$ [M-H]-	Peak area in urine (case #1) samples: $[M+H]^+$ $[M-H]^-$	
							with hydrolysis	without hydrolysis
A1	Nitroreduction	7.86	379.2484	-2.105	$C_{23}H_{30}N_4O$	4.7×10^5	4.7×10^5	5.7×10^5
A2	*O*-Deethylation + ketone formation (N-ethyl piperidinyl ring)	8.6	395.1708	-2.307	$C_{21}H_{22}N_4O_4$	-	3.0×10^5	3.1×10^5
A3	*O*-Deethylation + O-Glucuronidation	9.25	557.2235	-1.265	$C_{27}H_{32}N_4O_9$	-	1.40×10^5	1.2×10^7
A4	*O*-Deethylation + Hydroxylation (benzyl or ethoxyphenyl moiety)	9.74	397.1871	0.247	$C_{21}H_{24}N_4O_4$	1.40×10^5	-	-
A5	*O*-Deethylation + ketone formation (3-hydroxyphenyl moiety)	9.97	395.1709	-1.016	$C_{21}H_{22}N_4O_4$	6.00×10^6	-	-
A6	*O*-Deethylation + ketone formation (3-hydroxyphenyl moiety)	10.03	395.1714	0.046	$C_{21}H_{22}N_4O_4$	1.80×10^6	-	-
A7	*O*-Deethylation + Hydroxylation (N-ethyl piperidinyl ring)	10.06	397.1861	-2.346	$C_{21}H_{24}N_4O_4$	6.5×10^5	8.6×10^6	5.5×10^6
A8	*O*-Deethylation + Hydroxylation (3-hydroxyphenyl moiety)	10.38	397.1865	-1.213	$C_{21}H_{24}N_4O_4$	2.8×10^6	5.7×10^5	-
A9	*O*-Deethylation + Hydroxylation (benzyl or 3-hydroxybenzyl moiety)	10.47	397.1862	-2.044	$C_{21}H_{24}N_4O_4$	1.8×10^5	7.9×10^5	2.5×10^5

A10	*O*-Deethylation	11.6	381.1914	-1.908	$C_{21}H_{24}N_4O_3$	2.2x 10^7	3.7 x 10^6	2.3 x 10^6
A11	Hydroxylation (benzyl or ethoxyphenyl moiety)	14.54	425.2176	-1.627	$C_{23}H_{28}N_4O_4$	8.7 x 10^4	-	-
A12	*O*-Deethylation + ketone formation (benzyl or ethoxyphenyl moiety)	14.86	395.1709	-1.016	$C_{21}H_{22}N_4O_4$	5.6 x 10^5	-	-
A13	Hydroxylation (N-ethyl piperidinyl ring)	15.28	425.2177	-1.392	$C_{23}H_{28}N_4O_4$	2.2x 10^6	8.9 x 10^5	1.7 x 10^6
A14	Hydroxylation + *O*-glucuronidation	15.36	601.25	-0.681	$C_{29}H_{36}N_4O_{10}$	-	-	1.4 x 10^5
A15	N-Dealkylation + *O*-Glucuronidation	15.76	518.176	-1.603	$C_{24}H_{27}N_3O_{10}$	-	-	3.4 x 10^6
A16	Hydroxylation (*N*-ethyl piperidinyl ring)	15.76	425.2178	-1.039	$C_{23}H_{28}N_4O_4$	2.4 x 10^5	-	-
A17	Ring opening of *N*-substituted piperidine	16.03	441.2126	-1.465	$C_{23}H_{28}N_4O_5$	3.7 x 10^6	1.0 x 10^7	1.4 x 10^7
A18	Hydroxylation (benzyl or ethoxyphenyl moiety)	16.27	425.2176	-1.792	$C_{23}H_{28}N_4O_4$	9.5 x 10^5	4.2 x 10^5	-
A19	Ketone formation (3-hydroxyphenyl moiety)	16.36	423.202	-1.587	$C_{23}H_{26}N_4O_4$	1.8 x 10^5	-	-
A20	*O*-Deethylation + Oxidation (*N*-ethyl piperidinyl ring)	16.67	395.1706	-2.231	$C_{21}H_{22}N_4O_4$	4.2 x 10^5	4.1 x 10^7	4.6 x 10^6
	Parent (Etonitazepipne)	**16.76**	**409.2227**	**-1.582**	**$C_{23}H_{28}N_4O_3$**	**1.5 x 10^9**	**2.1 x 10^6**	**3.0 x 10^6**
A21	Hydroxylation (benzyl or ethoxyphenyl moiety)	17.04	425.2179	-0.922	$C_{23}H_{28}N_4O_4$	3.7 x 10^6	8.2 x 10^4	
A22	Ketone formation (3-hydroxyphenyl moiety)	18.77	423.2022	-1.091	$C_{23}H_{26}N_4O_4$	1.5 x 10^6		
A23	Ketone formation (N-ethyl piperidinyl ring)	19.67	423.2021	-1.209	$C_{23}H_{26}N_4O_4$	3.7 x 10^6	1.7 x 10^6	9.7 x 10^5

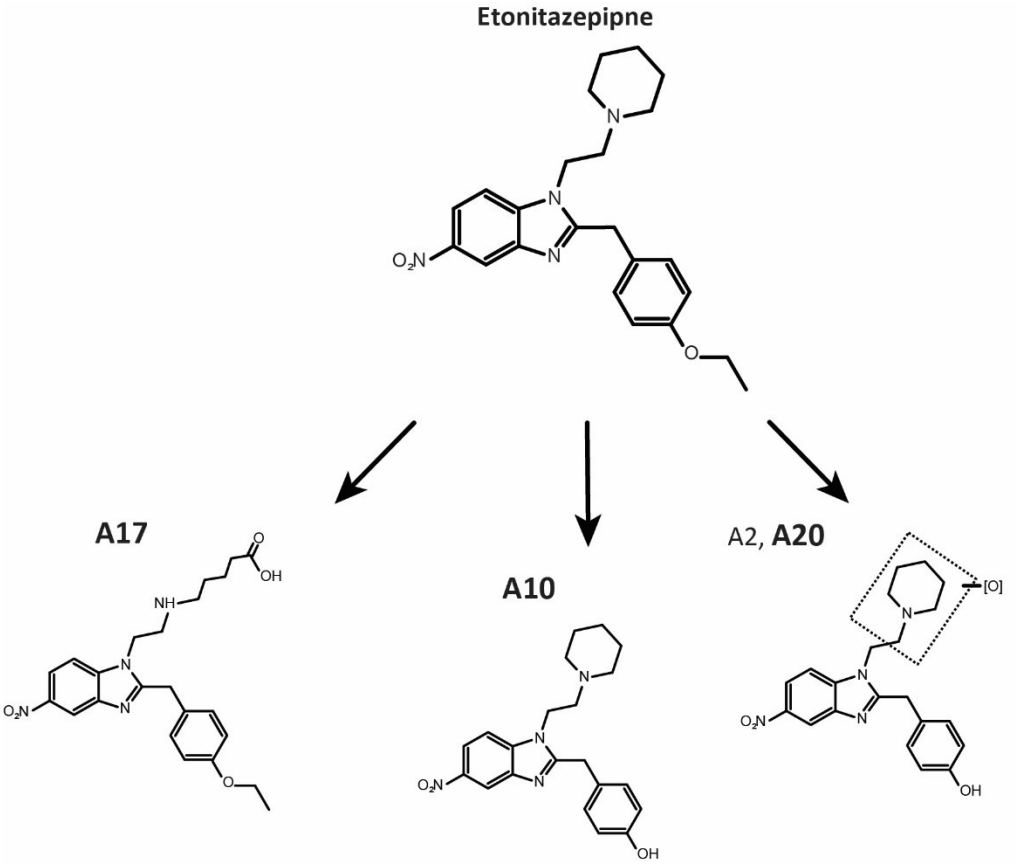


Figure 9: Proposed in vivo metabolic pathway of etonitazepipne

4.1.2. Etonitazepipne fragmentation pattern

Etonitazepipne fragmentation pattern is shown in Figure 10. Eluting at 16.79 min with *m/z* [M+H]+ 409.2228, etonitazepipne was detected both in the control (without pHLM), and in the post-mortem samples. As reported in literature (39,46), primary fragments observed were *m/z* 84.0808, 107.0492, 112.1121, and 135.0804, representing the piperidinyl ring, 3-hydroxybenzyl moiety, N-ethyl piperidinyl moiety, and ethoxy phenyl moiety.

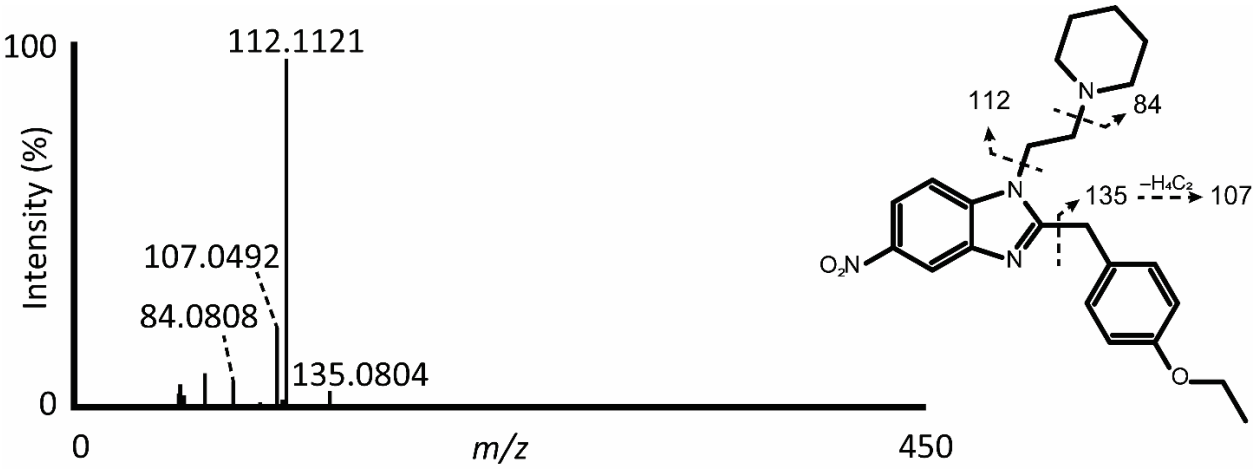


Figure 10: Etonitazepipne HR-MS/MS fragmentation pattern

A total of 24 and 15 metabolites were identified after 2 h incubation with pHLM and in the post-mortem after glucuronidase/arylsulfatase incubation, respectively.

4.1.2.1. *O*-Deethylation

A10 ($[M+H]^+$ *m/z* 381.1914, mass shift -28.031378 Da, differing by -C2H4 on its elemental composition from the parent) was the most abundant metabolite in the pHLM and second most prominent in the post-mortem hydrolyzed urine sample. Eluting at 11.602 min was generated after O-deethylation as suggested by the -28.0314 Da mass shift from the parent. The lack of the fragment ion at *m/z* 135 further supports this transformation (Fig. 11).

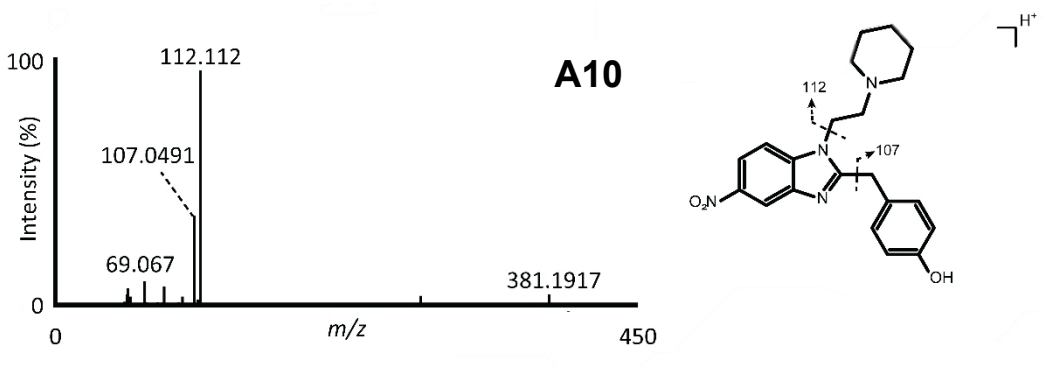


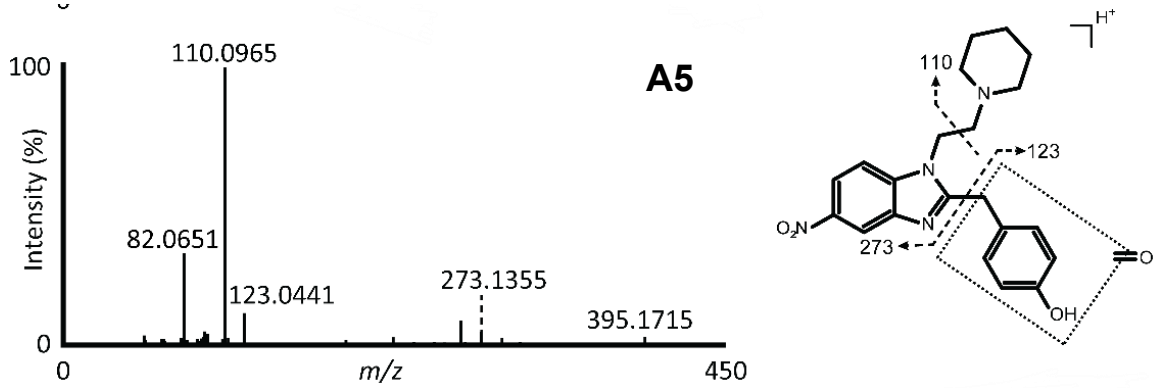
Figure 11: HR-MS/MS spectra of metabolite M10

4.1.2.2. *O*-Deethylation and ketone formation (or *N*-oxidation)

A5, with a protonated mass at *m/z* 395.171, was the second most abundant metabolite and was likely formed through N-deethylation and ketone formation, as indicated by the retention time at 9.797 min and a -14.0514 Da mass shift, reflecting a -C2H6+O difference in elemental composition compared to the parent drug (Fig. 12). The fragment ion at *m/z* 123 suggests that the transformation occurred at the 3-hydroxybenzyl moiety. A12 was produced by the same metabolic process, but different fragmentation spectra indicated that oxidation did not take place at the 3-hydroxybenzyl moiety. Despite diagnostic product ions at *m/z* 112 and 84 confirming the molecular structure, the exact position of the keto group could not be determined.

A6 had a different fragmentation pattern, where fragment *m/z* 123 indicates that the metabolic reaction occurred at the N-ethyl piperidinyl moiety. Moreover, A2 and A20 were generated by the same metabolic transformation and shared the same fragmentation spectra. The presence of fragment *m/z* 126 indicated that the keto formation occurred at the N-ethyl piperidinyl ring. Although A5, A6, and A12 were only detected in the incubates, A2 was detected in the urine sample and A20 in both pHLM and urine. A6 exhibited a distinct fragmentation pattern, with the fragment ion at *m/z* 123 indicating that the metabolic reaction occurred at the N-ethyl piperidinyl moiety. Additionally, A2 and A20 were generated through the same metabolic transformation and shared identical fragmentation spectra. The presence of the fragment ion at *m/z* 126 indicated that the keto group formation occurred at

the N-ethyl piperidinyl ring. While A5, A6, and A12 were exclusively detected in the incubates, A2 was found in the urine sample, and A20 was detected in both the



pHLM and urine samples.

4.1.2.3. Hydroxylation

A11, A13, A16, A18, and A21, with a protonated mass at *m/z* 425.2179 (+15.9952 Da mass shift), eluting at 14.536, 15.281, 15.763, 17.044 min, were generated by hydroxylation, as indicated by the +O shift in the elemental composition

Figure 12: HR-MS/MS spectra of metabolite A5

Hydroxylation occurred at the N-ethyl piperidinyl moiety for A13 and A16, with the fragment ion at *m/z* 128 suggesting the hydroxylation site. Fragmentation spectra for these metabolites did not show significant differences.

For A21 and A18, the primary fragments were *m/z* 98, 107, 110, and 135, with a slight modification for A21 at *m/z* 324. This indicated that the transformation likely occurred at the 2-nitrobenzimidazole moiety or the ethoxyphenyl moiety. A11 had only one diagnostic fragment at *m/z* 112, and the precise location of the hydroxylation could not be determined.

A13, A18, and A21 (Fig. 13) were identified in both pHLM and urine samples, while A11 and A16 were detected exclusively in the incubates.

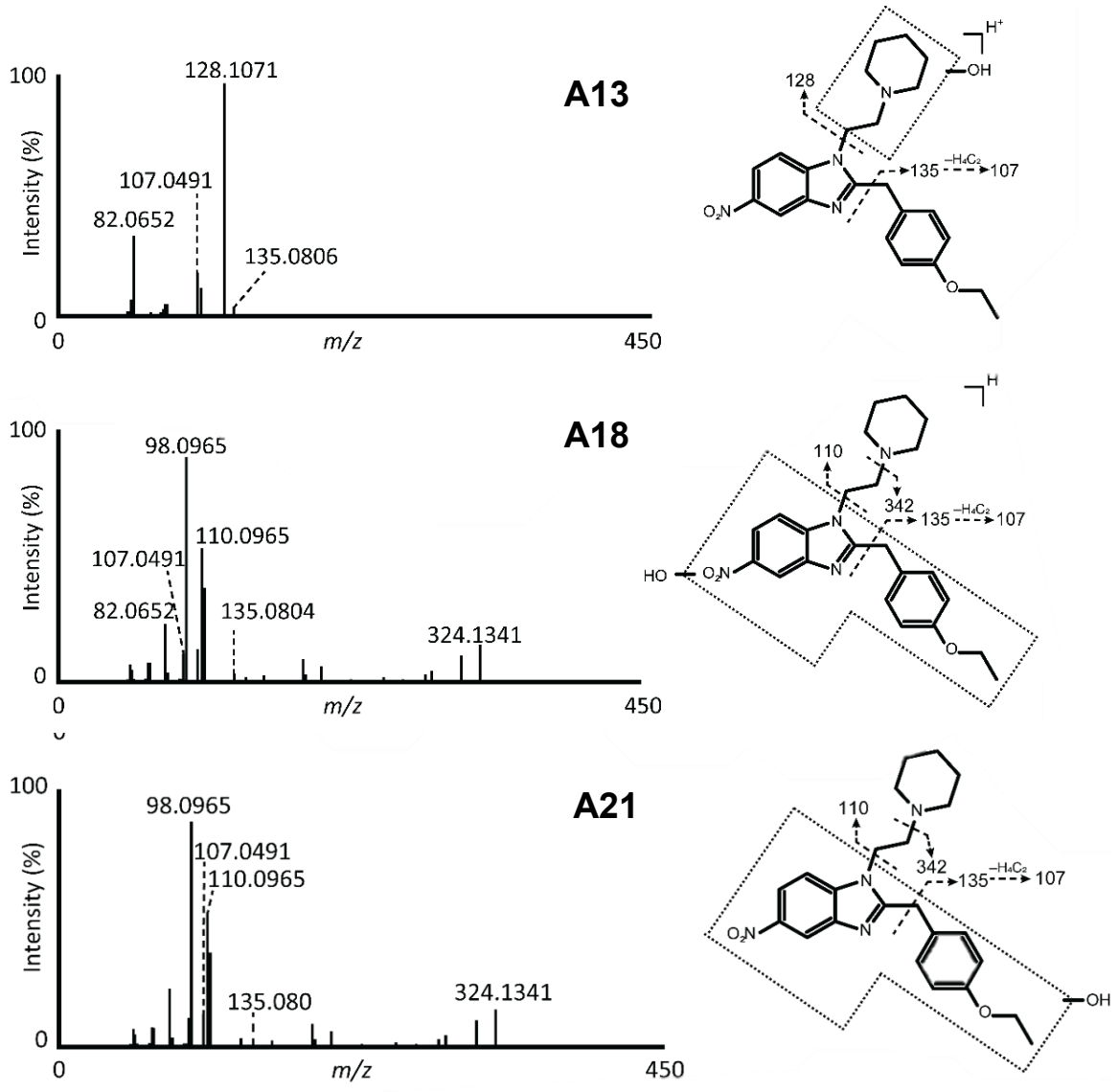


Figure 13: HR-MS/MS spectrum of metabolites A13, A18 and A21

4.1.3. *In vivo* Metabolites Identification

Etonitazepipne's *in vivo* metabolic profile was investigated through incubation with pHLM and analysis of post-mortem urine samples (Case #1). A total of 24 metabolites were identified after a 2-hour incubation with pHLM, while 15 metabolites were detected in the post-mortem samples following

glucuronidase/arylsulfatase treatment. The metabolites predominantly underwent Phase I transformations, including O-deethylation, hydroxylation, and ketone formation, with several compounds exhibiting distinct fragmentation patterns indicative of these processes.

4.1.4. Dipyanone metabolites identification in human hepatocytes

After incubating dipyanone with human hepatocytes, a total of eight metabolites were identified, including B1, B4, B5, B10, B12-14, and B15, listed by ascending retention time. Minor glucuronide conjugates (B2, B3, B6, B8, and B9) were also detected in the hepatocyte incubations, though their intensities were too low to be considered for identification.

However, B7 and B11 were not detected in hepatocyte incubations. Among the identified metabolites, B12 was the most abundant, likely resulting from ring opening and cyclisation, similar to the conversion of methadone to EDDP. B12 and B13 were the dominant metabolites.

Minor metabolites were formed via various processes, including hydroxylation of the phenyl ring, pyrrolidine ring, or alkyl chain, along with reduction and O-glucuronidation of B12. Table 6 details the elemental compositions, retention times, accurate masses, and LC-HRMS peak areas for dipyanone and its metabolites in positive ionisation mode following the three-hour incubation. Additionally, figure 14 and Figure 15 illustrates the extracted ion chromatograms of dipyanone and its

metabolites after the incubation period and its proposed metabolic pathway, respectively (44).

Table 6. Metabolic transformation, elemental composition, retention time (RT), accurate mass of molecular ion, deviation from theoretical accurate mass, and liquid chromatography-high-resolution mass spectrometry peak area of dipyanone and metabolites in positive ionisation mode after three hours of incubation with human hepatocytes and in postmortem samples.

ID	Biotransformation	Elemental composition	RT, min	*m/z* (*Δppm*)	**Hepatocytes**	**Urine #2a**		**Urine #2b**	
					Peak area	Peak area	Peak area with β-gluc	Peak area	Peak area with β-gluc
B1	Reduction & Hydroxylation (phenyl) & Hydroxylation (phenyl)	$C_{23}H_{31}NO_3$	6.55	370.2374 (-0.73)	9.6×10^5	1.6×10^8	1.8×10^8	1.2×10^8	1.1×10^8
B2	Hydroxylation (phenyl) & *O*-Glucuronidation	$C_{29}H_{37}NO_8$	6.78	528.2595 -0.58	$2.9 \times 10^{4**}$	ND	ND	5.2×10^8	ND
B3	Pyrr. op. to COOH & Cyclisation & *O*-Glucuronidation	$C_{30}H_{31}N_4O_4$	7.59	526.2441 -1.06	$1.0 \times 10^{4**}$	ND	ND	5.7×10^7	ND
B4	Pyrr. op. to butanol & Cyclisation & *O*-Glucuronidation	$C_{29}H_{37}NO_7$	7.61	512.2645 -0.43	5.0×10^5	5.5×10^8	ND	4.5×10^8	
B5	Hydroxylation (alkyl)	$C_{23}H_{29}NO_2$	7.67	352.2272 -0.27	8.5×10^5	ND	6.6×10^7	ND	ND
B6	Pyrr. op. to COOH & Cyclisation & *O*-Glucuronidation	$C_{29}H_{35}NO_8$	7.8	526.2444 -1.62	$3.4 \times 10^{4**}$	1.1×10^8	ND	1.7×10^8	6.9×10^7
B7	Pyrr. op. to butanol & Cyclisation	$C_{23}H_{29}NO_2$	7.81	352.2273 -0.55	ND	6.1×10^7	6.1×10^8	ND	4.6×10^7

	& Hydroxylation (butanol)								
B8	Hydroxylation (pyrr.) & *O*-Glucuronidation	$C_{29}H_{37}NO_8$	7.83	528.2592 -0.01	4.9 x 10^{4}**	1.3 x 10^{8}	ND	6.6 x 10^{7}	ND
B9	Hydroxylation (pyrr.) & *O*-Glucuronidation	$C_{29}H_{37}NO_8$	7.93	528.2529 -0.01	6.8 x 10^{4}**	1.2 x 10^{8}	ND	6.9 x 10^{7}	ND
B10	Hydroxylation (phenyl)	$C_{23}H_{29}NO_2$	7.98	352.2273 -0.05	7.3 x 10^{5}	ND	1.8 x 10^{8}	ND	6.8 x 10^{7}
B11	Hydroxylation (phenyl)	$C_{23}H_{29}NO_2$	8.11	352.2273 -0.05	ND	ND	ND	ND	5.9 x 10^{7}
B12	Pyrr. op. to butanol & Cyclisation	$C_{23}H_{29}NO$	8.25	336.23\2 (-0.27)	**1.8 x 10^{7}**	2.3 x 10^{9}	3.4 x 10^{9}	2.1 x 10^{9}	1.7 x 10^{9}
B13	Pyrr. op. to COOH & Cyclisation	$C_{23}H_{27}NO_2$	8.5	350.2119 -1.29	9.5 x 10^{6}	**5.4 x 10^{9}**	**5.7 x 10^{9}**	**5.6 x 10^{9}**	**3.3 x 10^{9}**
B14	Hydroxylation (pyrr.)	$C_{23}H_{29}NO_2$	8.57	352.2263 (-2.28)	3.8 x 10^{6}	ND	3.7 x 10^{8}	ND	3.5 x 10^{8}
	Dipyanone	$C_{23}H_{29}NO$	9.12	336.2318	7.7 x 10^{8}	1.1 x 10^{10}	1.3 x10^{10}	1.3 x10^{10}	8.0 x 10^{9}
B15	Hydroxylation (pyrr.)	$C_{23}H_{29}NO_2$	9.15	352.2266 (-1.43)	1.2 x 10^{6}	1.7 x 10^{6}*	8.9 x 10^{6}*	9.0 x 10^{6}*	8.4 x 10^{6}*

Mass tolerance, 5 ppm; gluc, glucuronide; NA, not applicable; ND, not detected; pyrr. op., pyrrolidine opening; *, found in authentic samples after identification in incubates; **, found retrospectively in incubates after identification in authentic samples

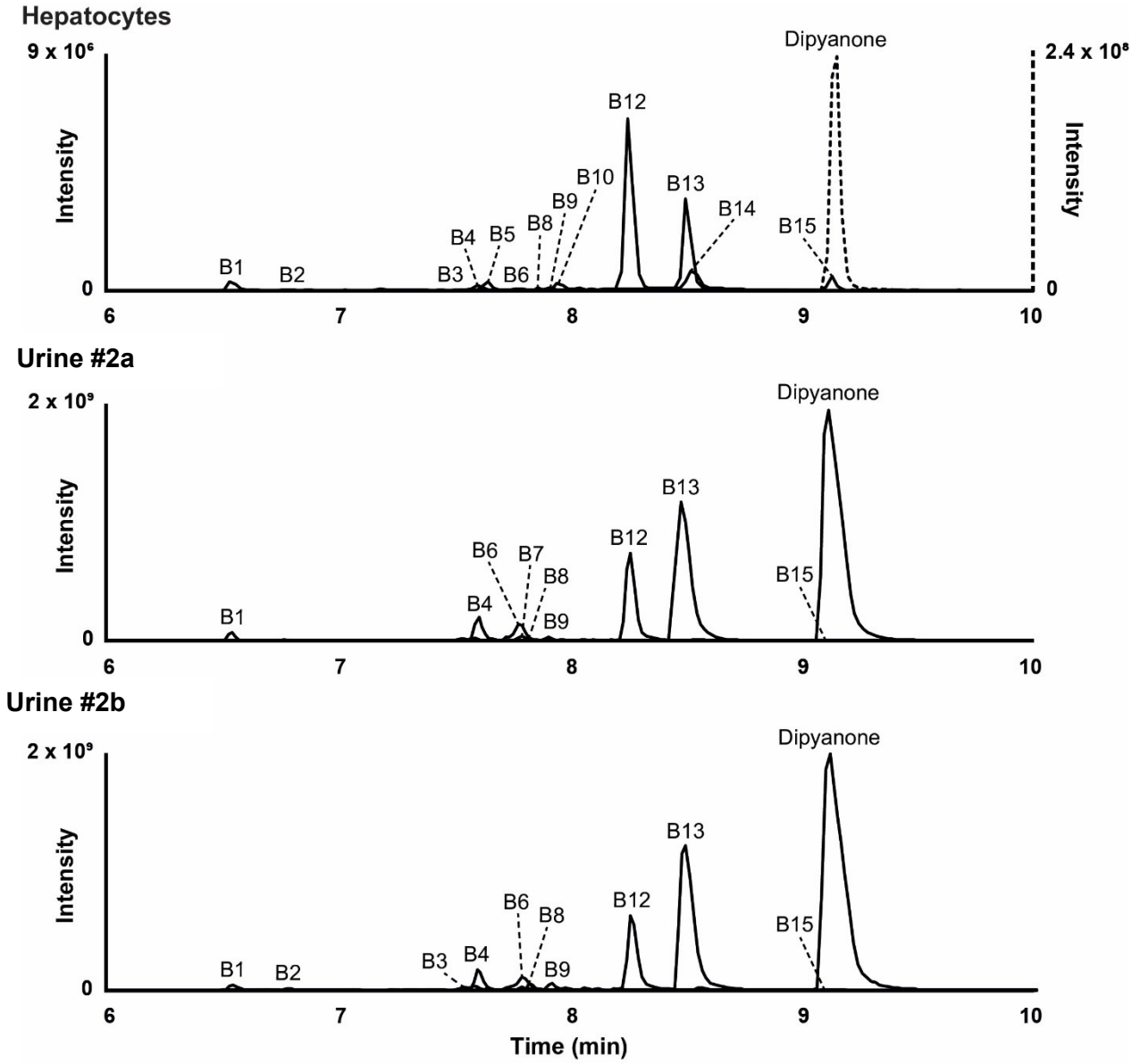


Figure 14: Extracted-ion chromatogram of dipyanone and metabolites in positive ionization mode of hepatocytes and urine case#1 and case#2. Mass tolerance, 5 ppm.

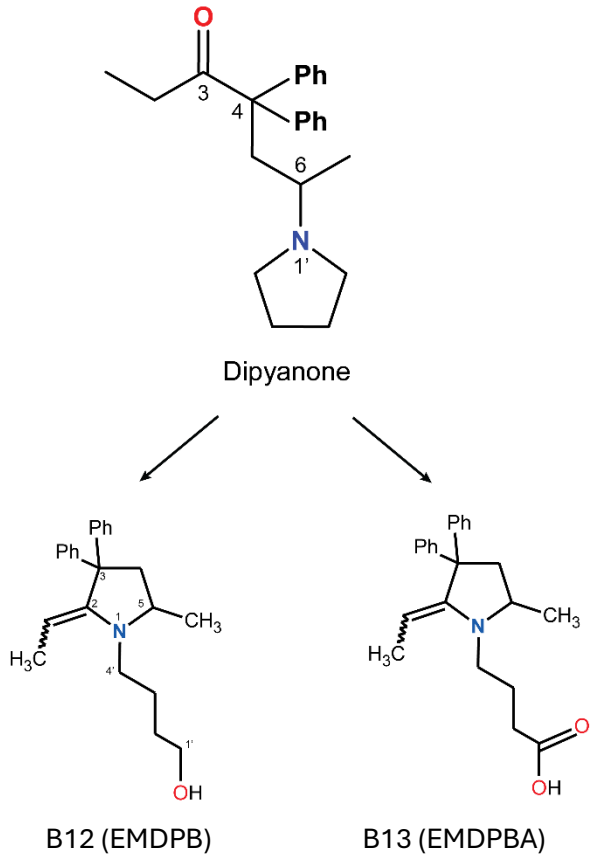


Figure 15: Dipyanone proposed metabolic pathway

4.1.5. Dipyanone Fragmentation Pattern

Dipyanone, with a protonated mass of $[M+H]^+$ at *m/z* 336.2335 (C23H30NO+), eluted at 9.13 min, and was not detected in negative ionisation mode. In line with previous literature, the fragmentation pattern of dipyanone revealed characteristic major fragments, primarily resulting from two key processes (15).

First, a pyrrolidine loss produced the fragment at *m/z* 265.1578 (C19H21O+), with a mass error of 3.3 ppm. The second process involved the loss of a propyl chain, generating a fragment at *m/z* 223.1125 ($C16H15O^+$) with a -3.6 ppm mass error. Other notable fragments included *m/z* 105.0337 ($C7H5O^+$) and *m/z* 91.0541 ($C7H7^+$), corresponding to the benzoyl and tropylium ions, respectively.

The complete dipyanone fragmentation spectra is shown in Figure 14. All metabolite signals and their corresponding fragments, unless otherwise specified, are described in positive ionisation mode (44).

4.1.5.1. Pyrrolidine ring opening and cyclisation

Metabolite B13 eluted at 8.50 min with a molecular ion at *m/z* 350.2119 ($C23H28NO2^+$), indicating the formation of an oxidized metabolite. B12, eluting at 8.25 min with *m/z* 336.2303 ($C23H30NO^+$), shares the same elemental composition as dipyanone. However, B12 and B13 produced distinctly different fragmentation spectra compared to dipyanone. While the HR-MS/MS spectrum of dipyanone primarily yields fragments containing oxygen atoms, B12 and B13 spectra are predominantly characterized by nitrogen-containing fragments. This suggests that B12 and B13 have structural differences from dipyanone.

Fragmentation analysis of B12 reveals a fragment at *m/z* 73.0650 ($C4H9O^+$), indicating a butanol chain cleavage, which suggests that the pyrrolidine ring was hydroxylated and subsequently opened. B13 exhibits a fragment at *m/z* 87.0438 ($C4H7O2^+$), indicating the loss of an alkyl chain with a terminal carboxyl group. Both B12 and B13 lose a butyl chain, leading to the same fragment at *m/z* 264.1757 ($C19H22N^+$), implying that B12 and B13 share the same scaffold but differ in their alkyl chains, B12 having a hydroxyl group and B13 a carboxyl group.

This observation suggests that dipyanone undergoes enzymatic hydroxylation at the α position of the pyrrolidine ring, forming an unstable cyclic hemiaminal intermediate. Hydroxylation at the β position would not result in an unstable intermediate that would lead to ring opening. The formation of B12 and B13 is reminiscent of the metabolic transformation of methadone to its primary metabolite, 2-ethylidene-1,5-dimethyl-3,3-diphenylpyrrolidine (EDDP). In both cases, ring opening results in a secondary amine that could perform a nucleophilic attack on the adjacent carbonyl carbon, forming a five-membered ring and a new hemiaminal. This intermediate could then undergo either ring opening or water loss, yielding the final structures of B12 and B13 (47–49). The intermediate metabolite (secondary amine with a butanal substituent) was not observed. Instead, following ring opening, the intermediate aldehyde is likely reduced to an alcohol or oxidized to a carboxylic acid, leading to the formation of B12 (4'-[2-ethylidene-5-methyl-3,3-diphenylpyrrolidin-1-yl]butan-1'-ol) and B13 (4'-[2-ethylidene-5-methyl-3,3-diphenylpyrrolidin-1-yl]butanoic acid). The fragmentation patterns of these metabolites are shown in Figure 16.

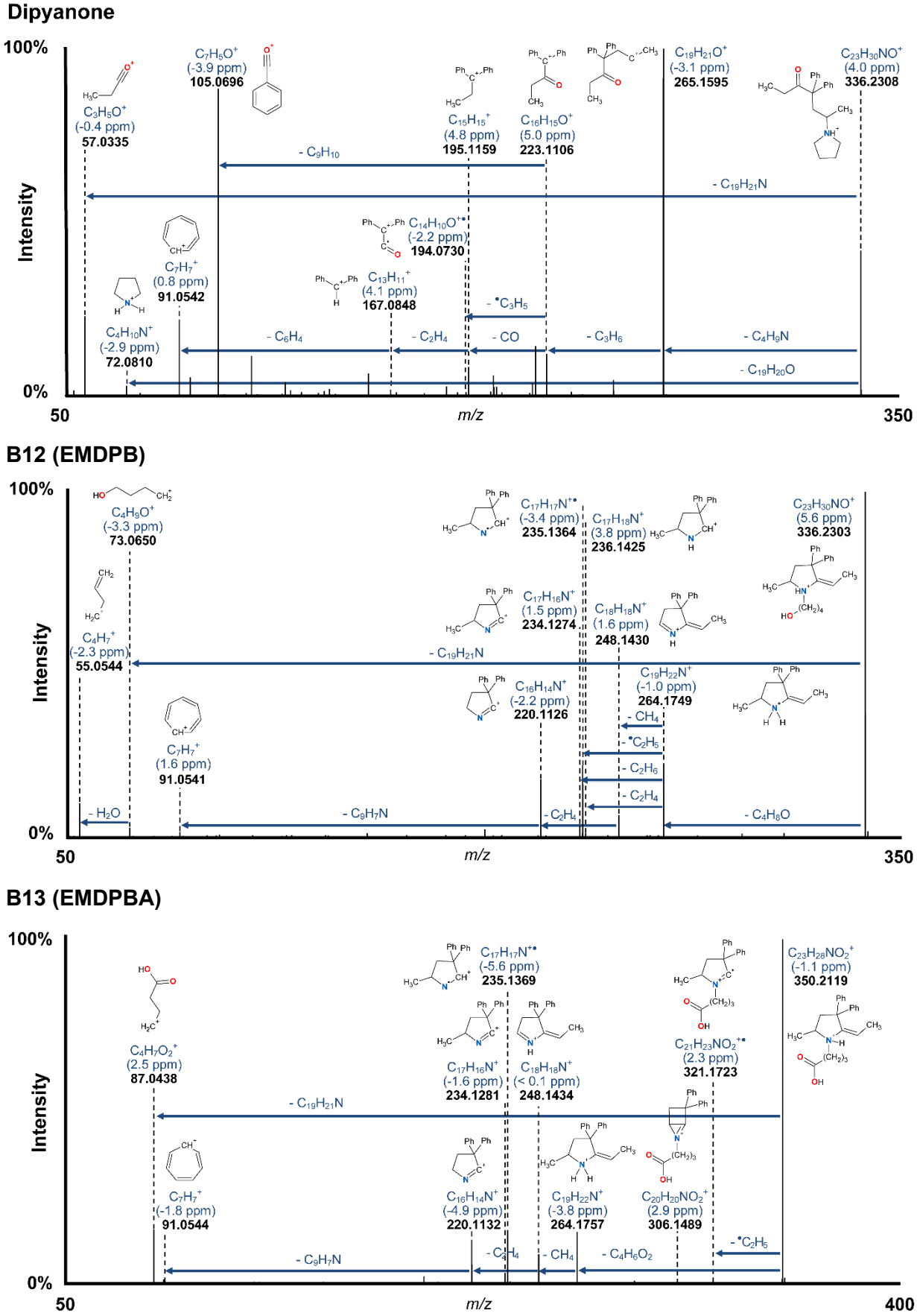


Figure 16: HR-MS/MS spectrum of dipyanone and main metabolites

4.1.5.2. *In vivo* Metabolites Identification

In case #2a, eight metabolites were initially identified in the urine sample (B1, B4, B6-9, B12, and B13). Following glucuronide hydrolysis, three additional metabolites (B5, B10, and B14) were detected. Similarly, case #2b revealed nine metabolites (B1-4, B6, B8, B9, B12, and B13) initially, and four more metabolites (B7, B10, B11, and B14) were detected after glucuronide hydrolysis. In both cases, B12 and B13 were the predominant metabolites, consistent with the results from the hepatocyte incubations. However, their relative proportions in the urine samples differed from those observed in the hepatocyte incubations, with B12 and B13 accounting for 23-26% and 61%, respectively, of the total metabolites' signal. Notably, the dipyanone signal was approximately twice as intense as B13, the principal metabolite. Glucuronide hydrolysis did not significantly increase the signal of the main metabolites. Both urine samples contained traces of B15, a minor hydroxylated metabolite previously observed *in vitro*, but its concentration was too low to be definitively identified. Table 1 summarizes the *in vivo* findings, and Figure 2 shows the extracted ion chromatograms of dipyanone and its metabolites in both urine samples (44).

4.1.6. Protonitazepyne & Metonitazepyne metabolites identification in human hepatocytes

After 3h incubation of protonitazepyne and metonitazepyne a total of 17 metabolites were identified for each compound (Table 7-8).

Both protonitazepyne and metonitazepyne exhibited similar metabolic patterns, with major transformations including pyrrolidine ring opening to butanoic acid, O-dealkylation, O-glucuronidation, oxidation, and hydroxylation. Minor metabolic reactions involved oxidation and nitro-reduction, N-oxidative deamination, O-dealkylation, and N,N-bis-dealkylation.

Metabolites detected below the established intensity threshold were excluded from the analysis. Detailed information on the metabolic transformations, elemental compositions, retention times, accurate masses of the molecular ions, deviations from theoretical accurate masses, and LC-HRMS/MS peak areas of metonitazepyne and protonitazepyne metabolites in both positive and negative ionization modes after 3-hour incubation with human hepatocytes can be found in Tables 7 and 8. Additionally, the extracted-ion chromatograms of metonitazepyne, protonitazepyne, and their metabolites after the 3-hour incubation, as well as real samples, are shown in Figure 17. In real samples, protonitazepyne was found to yield 10 metabolites (case #3, with and without hydrolysis).

Table 7: Metabolic transformation, elemental composition, retention time (RT), accurate mass of molecular ion, deviation from theoretical accurate mass, and liquid chromatography-high-resolution mass spectrometry peak area of protonitazepyne and metabolites in positive- and negative ionization mode after 3-h Incubation with human hepatocytes and in real samples.

ID	Biotransformation	Elemental composition	RT, min	*m/z* $[M+H]^+$ $[M-H]^-$	Mass error, (Δppm)	Peak area in incubates: $[M+H]^+$ $[M-H]^-$	Peak area in blood sample: $[M+H]^+$ $[M-H]^-$	Peak area in urine (case #3) samples: $[M+H]^+$ $[M-H]^-$	
								without hydrolysis	with hydrolysis
C1	*O*-Dealkylation + Sulfation	$C_{20}H_{22}N_4O_6S$	3.27	447.1340 ND	1.61 -	4.89×10^6 ND	ND ND	ND ND	ND ND
C2	*O*-Deethylation + *O*-Glucuronidation	$C_{26}H_{31}N_4O_9$	8.38	543.2084 541.1943	-0.28 0.55	6.36×10^7 3.13×10^7	ND ND	2.56×10^7 9.37×10^6	ND ND
C3	Nitro reduction	$C_{23}H_{30}N_4O$	8.70	379.2492 ND	-0.10 -	$2.3 \times 10^{6*}$ -	6.7×10^6 -	3.52×10^6 -	4.5×10^6 -
C4	*N*-Oxidative deamination + O-Dealkylation + Gluc	$C_{22}H_{23}N_3O_{10}$	9.29	490.1459 ND	0.57 -	3.61×10^6 -	ND ND	ND ND	ND ND
C5	Pyrrolidine ring opening to butanoic acid + *O*-Dealkylation	$C_{20}H_{23}N_4O_5$	9.85	399.1662 397.1532	-0.24 3.67	9.64×10^6 3.78×10^6	ND ND	ND ND	ND ND
C6	*O*-Deethylation	$C_{20}H_{23}N_3O_4$	10.52	367.1765 ND	0.09 -	1.80×10^7 ND	ND ND	2.24×10^6 ND	5.20×10^7 ND
C7	*N*-Oxidative deamination + *O*-Dealkylation	$C_{16}H_{15}N_3O_4$	12.04	314.1129 312.0994	-2.01 1.35	1.37×10^7 4.23×10^6	ND ND	9.81×10^5 ND	9.43×10^6 ND
C8	Pyrrolidine ring opening to *N*-butanoic acid + Hydroxylation	$C_{23}H_{29}N_4O_6$	12.04	457.2075 ND	-1.45 -	1.52×10^7 ND	ND ND	4.72×10^6 ND	4.23×10^6 ND

C9	O-Dealkylation + Oxidation + Gluc	$C_{26}H_{28}N_4O_{10}$	12.32	557.1881 ND	0.50 -	2.6 x 10^6 -	ND ND	ND ND	ND ND
C10	Hydroxylation (where)	$C_{23}H_{29}N_4O_4$	12.56	425.2185 ND	0.39 -	2.61 x 10^7 ND	ND ND	3.55 x 10^6 ND	3.51 x 10^6 ND
C11	Oxidation (pyrrolidine) + Nitro reduction	$C_{23}H_{29}N_4O_2$	14.69	393.2287 ND	0.50 -	2.45 x 10^7 ND	3.29 x 10^6 ND	2.91 x 10^6 ND	3.73 x 10^6 ND
C12	*O*-Dealkylation + Oxidation (where)	$C_{20}H_{20}N_4O_4$	15.35	381.1558 ND	0.18 -	8.90 x 10^6 ND	ND ND	ND ND	5.52 x 10^6 ND
C13	*N*,*N*-Didealkylation	$C_{19}H_{23}N_4O_3$	16.29	355.1766 ND	0.37 -	1.82 x 10^7 ND	ND ND	ND ND	ND ND
C14	*N*-Glucuronidation	$C_{29}H_{37}N_4O_9$	16.46	585.2558 ND	0.50 -	9.48 x 10^6 ND	ND ND	ND ND	ND ND
C15	Hydroxylation (Pyrrolidine)	$C_{23}H_{29}N_4O_4$	16.62	425.2181 ND	-0.54 -	2.61 x 10^7 ND	ND ND	ND ND	ND ND
C16	Pyrrolidine ring opening to *N*-butanoic acid	$C_{23}H_{29}N_4O_5$	16.75	441.2123 439.1993	-2.14 1.38	3.22 x 10^8 1.42 x 10^8	1.06 x 10^5 6.05 x 10^4	2.92 x 10^7 ND	2.64 x 10^7 5.69 x 10^6
Parent	**Protonitazepyne**	**$C_{23}H_{29}N_4O_3$**	**17.26**	**409.2224 ND**	**-2.49 -**	**3.42 x 10^8 ND**	**1.18 x 10^6 ND**	**1.38 x 10^7 ND**	**8.72 x 10^6 ND**
C17	Oxidation (pyrrolidine)	$C_{23}H_{27}N_4O_4$	19.78	423.2022 ND	-1.14 -	9.79 x 10^7 ND	5.98 x 10^5 ND	7.93 x 10^5 ND	7.78 x 10^5 ND

Table 8: Metabolic transformation, elemental composition, retention time (RT), accurate mass of molecular ion, deviation from theoretical accurate mass, and liquid chromatography-high-resolution mass spectrometry peak area of metonitazepyne and metabolites in positive- and negative- ionization mode after 3-h Incubation with human hepatocytes.

ID	Biotransformation	Elemental composition	RT (min)	*m/z* $[M+H]^+$ $[M-H]^-$	Mass error, Δppm	Peak area at T_{3h}
D1	Nitro-reduction	$C_{21}H_{26}N_4O$	4.84	351.2180 ND	0.18 -	3.53×10^6 ND
D2	Oxydation (pyrrolidine) + *O*-Dealkylation + Nitro reduction	$C_{20}H_{23}N_4O_2$	6.89	351.1816 ND	0.13 -	1.16×10^6 ND
D3	*O*-Dealkylation + *O*-Glucuronidation	$C_{26}H_{31}N_4O_9$	8.37	543.2083 541.1957	-0.65 3.14	2.06×10^7 9.36×10^6
D4	Hydroxylation (where) + *O*-Glucuronidation	$C_{27}H_{32}N_4O_{10}$	8.81	573.2195 ND	0.66 -	5.71×10^5 ND
D5	Hydroxylation (pyrrolidine) + *O*-Dealkylation	$C_{20}H_{23}N_4O_4$	9.57	383.1714 ND	0.05 -	3.07×10^6 ND
D6	N-Dealkylation to butanoic acid + *O*-Dealkylation	$C_{20}H_{23}N_4O_5$	9.82	399.1660 397.1533	-0.74 3.67	1.08×10^7 4.31×10^6
D7	Oxydation (pyrrolidine) + Nitro reduction	$C_{21}H_{25}N_4O_2$	10.44	365.1974 ND	0.54 -	1.06×10^7 ND
D8	*O*-Dealkylation	$C_{20}H_{23}N_4O_3$	10.49	367.1765 365.1631	0.09 2.97	1.95×10^7 3.61×10^6
D9	N-Oxidative deamination + O-Dealkylation	$C_{16}H_{15}N_3O_4$	12.01	314.1128 -	-2.33 -	7.41×10^6 ND

D10	Hydroxylation (where) + *O*-Glucuronidation	$C_{27}H_{32}N_4O_{10}$	12.14	573.2181	-1.78	1.80×10^6 ND
D11	*N*,*N*-Didealkylation	$C_{17}H_{18}N_4O_3$	12.25	327.1447 ND	-1.43 -	4.29×10^6 ND
D12	Hydroxylation (pyrrolidine)	$C_{21}H_{25}N_4O_4$	13.12	397.1865 ND	-1.34 -	6.31×10^7 ND
D13	Pyrrolidine to butanoic acid	$C_{21}H_{25}N_4O_5$	13.46	413.1813 411.1683	-1.56 2.21	8.47×10^7 2.96×10^7
Parent	**Metonitazepyne**	**$C_{21}H_{25}N_4O_3$**	**14.28**	**381.1912 ND**	**-2.41 -**	**2.25×10^8 ND**
D14	Pyrrolidine opening to butanal	$C_{21}H_{25}N_4O_4$	14.39	399.2024 ND	0.35 -	6.2×10^5
D15	Hydroxylation (where)	$C_{21}H_{25}N_4O_4$	14.85	397.1872 ND	0.42 -	9.44×10^6 ND
D16	Oxydation (pyrrolidine) + *O*-Dealkylation	$C_{20}H_{21}N_4O_4$	15.33	381.1561 ND	0.97 -	1.17×10^7 ND
D17	Oxydation (pyrrolidine)	$C_{21}H_{23}N_4O_4$	17.99	395.1706 ND	-1.98 -	7.05×10^7 ND

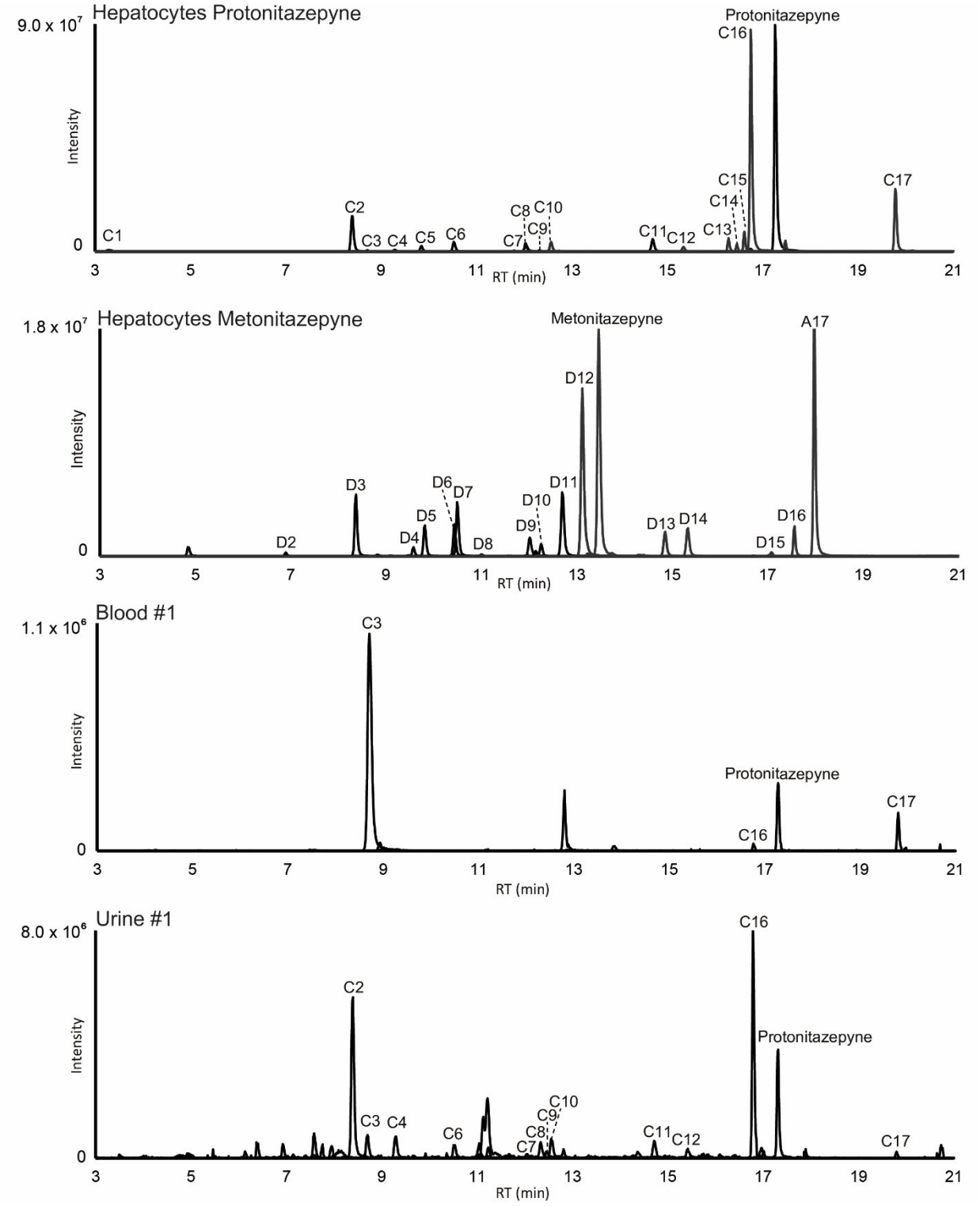


Figure 17: : Extracted-ion chromatogram of protonitazepyne and metonitazepyne and metabolites in positive ionization mode of hepatocytes and urine case#1 and blood case#1. Mass tolerance, 5 ppm.

4.1.7. Protonitazepyne and Metonitazepyne Fragmentation Pattern

Protonitazepyne exhibited a base peak at *m/z* 409.2224 with a retention time of 17.26 minutes. Consistent with its structural analogues, the fragmentation pattern revealed key fragments at *m/z* 98.0963 and 107.0490, which correspond to the N-methyl pyrrolidine and hydroxybenzyl moieties, respectively (Figure 16). The primary metabolic transformations observed for protonitazepyne were N-dealkylation to butanoic acid, oxidation, and hydroxylation.

Metonitazepyne, on the other hand, eluted at 14.28 minutes with a base peak at *m/z* 381.1912. The fragmentation spectrum of metonitazepyne presented a prominent fragment at *m/z* 121.0645, which corresponds to the methoxybenzyl fragment, as previously reported by Taoussi et al. (29). In addition to this, the most characteristic fragment observed was at *m/z* 98.0962, which represents the N-methyl pyrrolidine moiety (Figure 18). The primary transformations for metonitazepyne were similar, including N-dealkylation to butanoic acid, oxidation, and hydroxylation (45).

4.1.7.1. *N*-dealkylation to butanoic acid

N-dealkylation to butanoic acid was identified as the most prominent metabolic transformation in hepatocytes for both protonitazepyne (C16, [M+H]+ 441.2123 ±5 ppm, RT 16.75 min) and metonitazepyne (D13, [M+H]+ 413.1813 ±5 ppm, RT 13.46 min) (Figures 18 and 19). The observed mass shift of 31.990 Da ±5 ppm from the parent compound strongly suggested this transformation. Key fragments detected for both analogues included *m/z* 69.0334, 87.0439, 130.0860, and 176.0452

±5 ppm. The fragment at *m/z* 87.0439 ±5 ppm corresponded to the butanoic acid moiety, confirming the N-dealkylation process. Additionally, the fragment at *m/z* 284.2022 ±5 ppm, representing the methoxyphenyl-methyl-nitrobenzimidazole, was observed in metonitazepyne, while the fragment at *m/z* 312.1336, corresponding to the propoxyphenyl-methyl-nitrobenzimidazole moiety, was detected in protonitazepyne.

4.1.7.2. Oxidation

C17 and D17 were the second most intense metabolites detected in human hepatocytes, formed through oxidation at the pyrrolidine ring (-H2O). For metonitazepyne, metabolite D17 eluted at 17.99 min with a base peak at *m/z* 395.1706 ±5 ppm. For protonitazepyne, metabolite C17 was detected at 19.78 min with a base peak at *m/z* 423.2022 ±5 ppm. A mass shift of 13.9799 Da was observed for both metabolites, and they exhibited the same fragmentation pattern. The main fragments included *m/z* 69.0334, 84.0806, and 112.0754 ±5 ppm, which were attributed to the water loss from the pyrrolidine moiety, the oxo-pyrrolidine ring, and the ethyl-oxo-pyrrolidine ring, respectively (Figures 18 and 19).

4.1.7.3. Hydroxylation

Metabolites D12 ([M+H]+ 397.1865 ±5 ppm, RT 13.12 min) and C10 ([M+H]+ 425.2185 ±5 ppm, RT 12.56 min) were formed after hydroxylation. For metonitazepyne, the fragmentation pattern of D12 showed a characteristic fragment at *m/z* 114.0911 ±5 ppm, indicating that hydroxylation occurred at the pyrrolidine

ring. A further fragment at *m/z* 96.0805 was observed, resulting from the loss of water from *m/z* 114.0911. In contrast, protonitazepyne metabolite C10 exhibited a different fragmentation profile, with the main fragments at *m/z* 98.0963 and 107.0490. These fragments did not provide clear information regarding the specific position of the hydroxyl group (Figures 18 and 19).

4.1.7.4. *O*-dealklation and *O*-glucuronidation

The second-phase transformation of metonitazepyne and protonitazepyne produced metabolites C2 and D3 ([M+H]+ 543.2083 ±5 ppm, RT 8.37 min) through O-dealkylation and O-glucuronidation. Both metabolites, C2 and D3, shared the same fragmentation pattern, with characteristic fragments at *m/z* 98.0962 and 107.0489 ±5 ppm, as previously described. Additionally, fragment *m/z* 367.1757 ±5 ppm was observed, representing the loss of the glucuronide group (Figures 18 and 19).

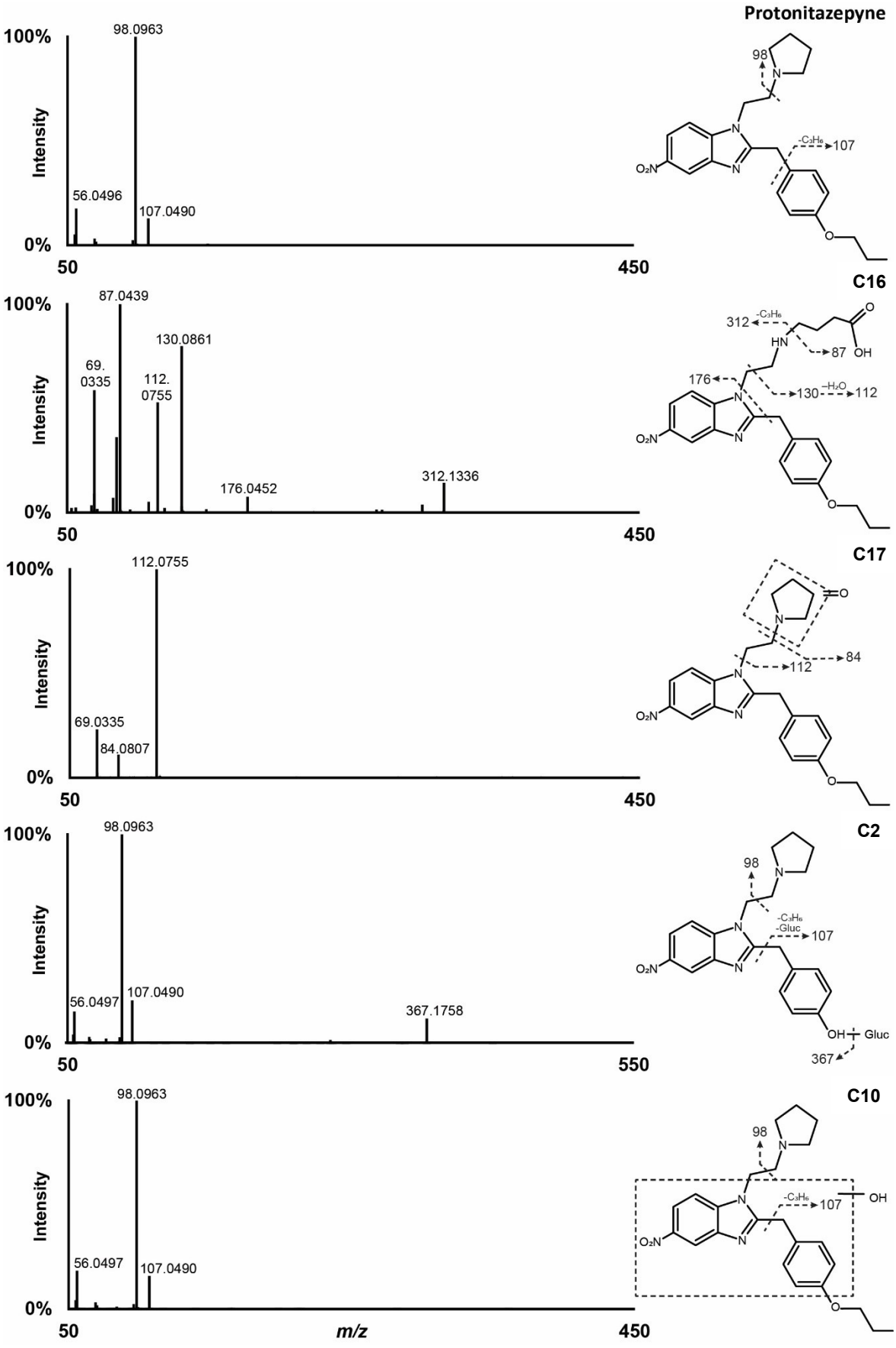


Figure 18: HR-MS/MS spectrum of protonitazepyne and main metabolites

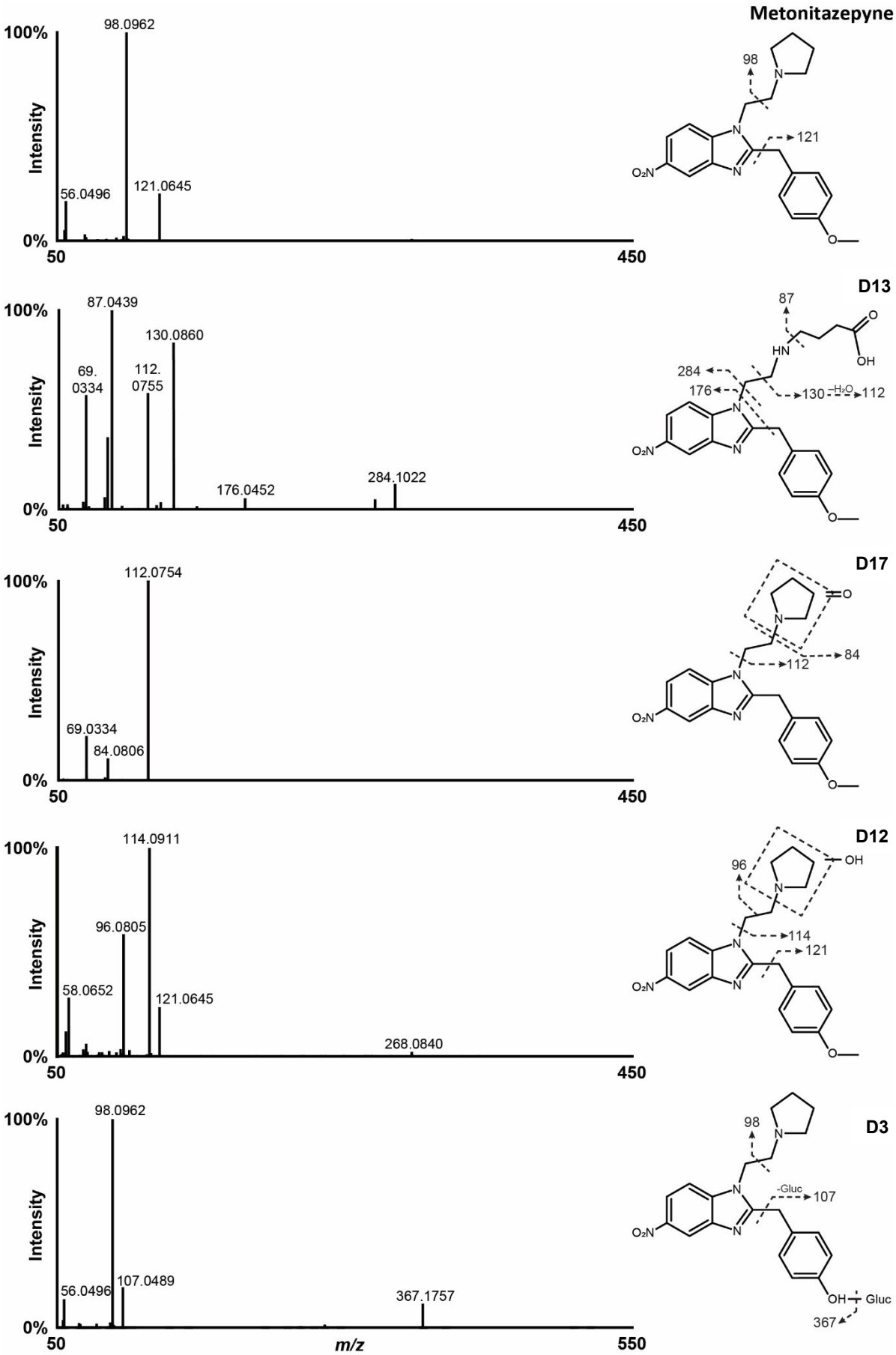


Figure 19: HR-MS/MS spectrum of metonitazepyne and main metabolites

4.1.8. *In vivo* Metabolite Identification

Blood and urine samples (Case #3) positive for protonitazepyne were analysed (Table 8). In comparison to hepatocyte incubations, which yielded 18 metabolites, a total of 5 metabolites were detected in the blood sample, and 10 metabolites were detected in the urine sample. As with the hepatocyte results, the most intense metabolites in both blood and urine were pyrrolidine ring opening to N-butanoic acid (C16) and O-dealkylation & O-glucuronidation (C2). Further hydroxylation of D16 produced metabolite C8 ($[M+H]^+$ 457.2075 ±5 ppm, RT 12.04 min), which was the third most intense metabolite in urine. Additionally, metabolite C10 was found to be a major metabolite in urine, though it was absent in the blood sample. Metabolite C3, produced after nitro reduction ($[M+H]^+$ 379.2492 ±5 ppm, RT 8.70 min), was prominent in both the blood and urine samples. Interestingly, this metabolite was retrospectively detected in the hepatocyte incubations after being identified in the real samples (45).

4.2. MOR, KOR, and DOR *in vitro* activation profiles

4.2.1. Etonitazepipne

Etonitazepipne *in vitro* activation profile at MOR, DOR and KOR are displayed in figure 20-22. In line with published literature (39), at MOR, etonitazepipne presented an EC_{50} of 9.4 nM, and E_{max} of 143%, which resulted in a strong MOR activity, around 3 times more potent than fentanyl and higher efficacy.

At KOR and DOR, etonitazepipne was relatively less potent than at MOR, with an EC_{50} of 3042 and 3215 nM, respectively; as well as E_{max} that did not exceed 25% in both receptors. Although, a recent study from Baumann et al, describes the pharmacological activity at the 3 receptors using a radioactive-assay, results were consistent with our findings (50).

4.2.2. Dipyanone

The *in vitro* activation profiles of the MOR, KOR, and DOR, represented by the normalized FRET signal intensity based on the concentration of dipyanone and controls, are shown in Figure 20-22. The EC_{50} and E_{max} values for dipyanone at these receptors are detailed in Table 9.

Dipyanone demonstrated strong potency at MOR (EC_{50}, 96.8 nM), but its potency was four to five times lower than that of fentanyl. Its efficacy was similar to fentanyl. At KOR and DOR, dipyanone showed significantly reduced potency (EC_{50}, 380 nM and 1067 nM, respectively) and efficacy (E_{max}, 13% and 56%, respectively). This selective receptor activation profile is comparable to that of methadone, supporting previous studies that suggest dipyanone shares similar analgesic and toxicity profiles with methadone (15,44).

4.2.3. Protonitazepyne and metonitazepyne

In vitro receptor activation of metonitazepyne and protonitazepyne at MOR, KOR and DOR receptors is displayed in Fig. 20-22.

Protonitazepyne exhibited full activation at MOR, with an EC_{50} of 3.7 nM (2.2-8.7 nM), which was approximately 8-9 times more potent than fentanyl (EC_{50} = 25.6 nM, 10.7-70.2 nM). Metonitazepyne also showed increased potency, with an EC_{50} of 11.5 nM (6.8-14.6 nM), making it roughly three times more potent than fentanyl. These results align with those reported by Kozell et al. (50), where protonitazepyne and metonitazepyne exhibited similar high potencies at MOR with EC_{50} values in the low nanomolar range (0.30 and 18.2 nM, respectively). De Vrieze et al. (19) also reported enhanced MOR activation for protonitazepyne and metonitazepyne, surpassing traditional opioids like fentanyl (0.9 and 12.0 nM, respectively).

Furthermore, protonitazepyne demonstrated an E_{max} of 154%, indicating a more efficacious MOR activation compared to fentanyl, arbitrarily set at 100%. Metonitazepyne showed an E_{max} of 101%, comparable to fentanyl. These findings confirm that both protonitazepyne and metonitazepyne are more potent and efficacious at MOR than fentanyl, consistent with previously published data on novel synthetic opioids (19,50)

At KOR, protonitazepyne exhibited low to no activation, with an EC_{50} of 2529.1 nM and an E_{max} of 14%, compared to the reference U-50488. Metonitazepyne was slightly more potent, with an EC_{50} of 256.7 nM and an E_{max} of 22%, though both compounds showed limited activation compared to U-50488. Table 9 summarizes the *in vitro* activation data for MOR, KOR, and DOR. These findings are consistent

with data from Kozell et al., suggesting that these compounds have limited activity at KOR and DOR compared to their significant activation of MOR (50).

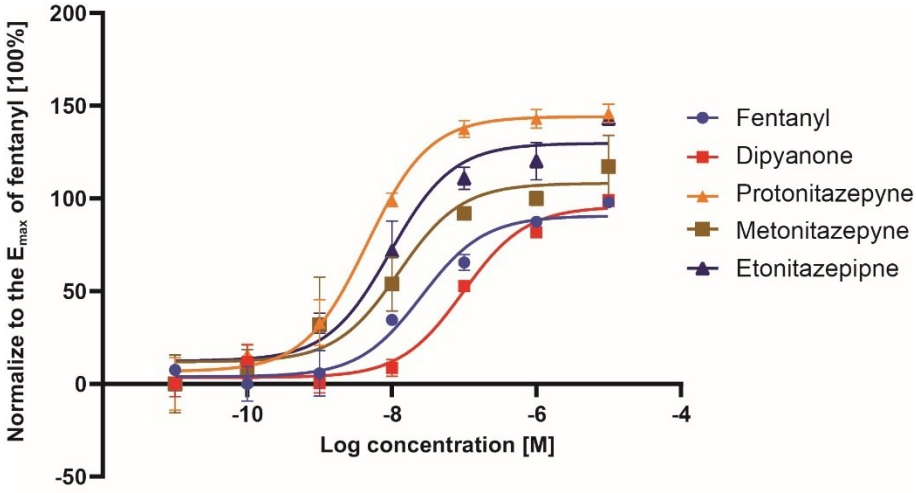


Figure 20 Agonist pharmacological characterisation of Etonitazepipne, Dipyanone, Proto- and Metonitazepyne at MOR.

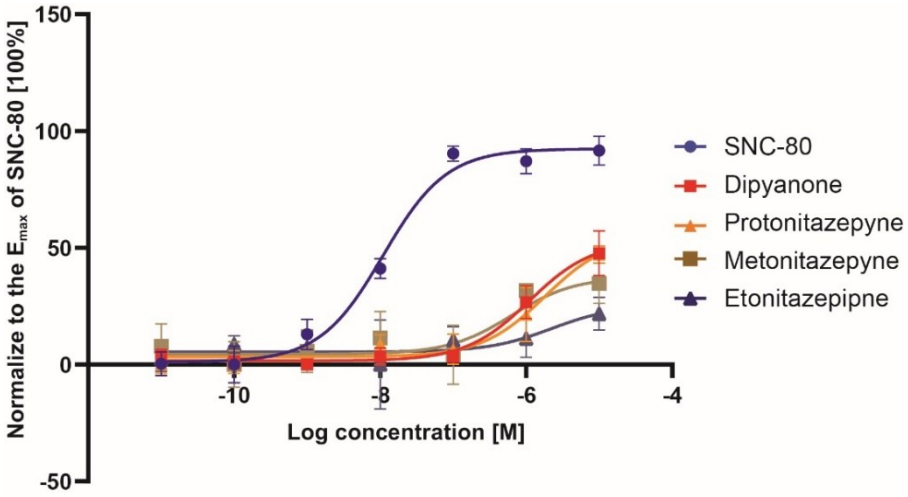


Figure 22:Agonist pharmacological characterisation of Etonitazepipne, Dipyanone, Proto- and Metonitazepyne at DOR.

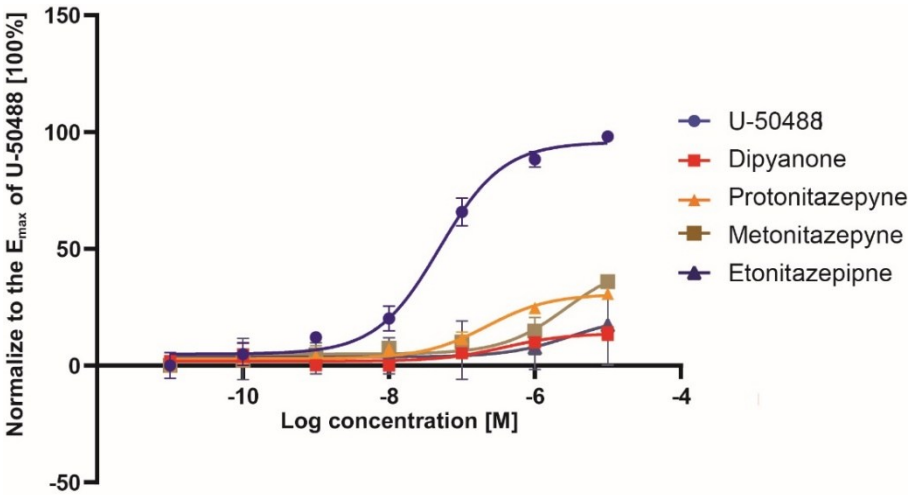


Figure 21: Agonist pharmacological characterisation of Etonitazepipne, Dipyanone, Proto- and Metonitazepyne at KOR.

Table 9. *In vitro* MOR, KOR, and DOR activation using a HTRF®GTP Gi binding assay, represented by their potency (EC_{50}) and efficacy (E_{max}) values (relative to fentanyl [MOR], U-50488 [KOR], SNC-80 [DOR]). 95% confidence intervals are given between parentheses. *Max activation could not be reached.

Compound	MOR		KOR		DOR	
	EC_{50} [nM]	E_{max} [%] relative to fentanyl	EC_{50} [nM]	E_{max} [%] relative to U-50488	EC_{50} [nM]	E_{max} [%] relative to SNC-80
Fentanyl	25.6 (10.1- 70.2)	100 (98-119)	-	-	-	-
U-50488	-	-	49.4 (29.6-80.1)	100 (98-113)	-	-
SNC-80	-	-	-	-	4.5 (2.1-9.7)	100 (89-108)
Etonitazepipne	9.4 (2.3-48.2)	143 (133-185)	3042*	17*	3215*	25*
Dipyanone	96.8 (51.6-181.2)	106 (98-121)	380.4 (36.9-511.6)	13 (10-24)	1067 (516-1812)	56 (45-75)
Protonitazepyne	3.7 (2.2-8.7)	154 (152-186)	2530 (2311.2-2781.5)	14 (10-24)	424.7 (202.3-790.5)	56 (54-72)
Metonitazepyne	11.5 (6.8-14.6)	101 (84-120)	256.7 (196.9-311.6)	22 (16-33)	265.8 (96.8-742.7)	36 (30-46)

5. Discussion

5.1. NSO metabolic profiling

5.1.1. Etonitazepipne metabolism

The pHLM assay and analysis of the urine sample (both before and after glucuronide/arylsulfatase cleavage) identified a total of 20 and 14 metabolites, respectively. Moreover, 3 phase II metabolites were detected in the real samples. O-deethylation were the major metabolization pathway of etonitazepipne (39). However, the metabolite formed after O-dealkylation and piperidine contraction, which was reported by Vandeputte et al. (39), was not observed in our analysis. Additionally, one of the most intense metabolites detected after hydrolysis in our study (M17, a ring opening of N-substituted piperidine) was not mentioned in the publication by Vandeputte et al. Ring opening of a pyrrolidine or piperidine moieties is a common metabolic reaction in molecules carrying these functional groups (39). As anticipated, the parent compound etonitazepipne was the most abundant in the *in vitro* assay, followed by metabolites M10 (O-dealkylation) and M5 (O-dealkylation and oxidation). In the urine sample, the most abundant metabolites were M20 (O-dealkylation and oxidation) and M10 (O-dealkylation). Out of the 19 metabolites detected *in vitro*, only 12 were confirmed by the analysis of the authentic urine sample. Other less intense transformations detected included hydroxylation, O-dealkylation, and combined O-dealkylation and nitro reduction for both pHLM and the urinary matrix.

5.1.2. Dipyanone metabolism

A strong correlation was observed between *in vitro* and *in vivo* findings.

The primary metabolites identified in hepatocyte incubations, EMDPB (M12) and EMDPBA (M13), were also the predominant metabolites detected in urine samples positive for dipyanone. These findings suggest that EMDPB and EMDPBA could serve as reliable biomarkers for dipyanone use.

In terms of signal intensity, dipyanone was approximately four times more abundant than EMDPB and twice as abundant as EMDPBA in both urine samples. Notably, enzymatic hydrolysis of urine samples did not increase the signal intensity of EMDPB or EMDPBA.

A study by Bernard et al. demonstrated that methadone excretion in urine depends on pH, whereas EDDP excretion does not (51). At a pH below 5.5, methadone and EDDP concentrations were similar, but as the pH increased, the methadone-to-EDDP concentration ratio decreased. It remains unclear whether a similar pH-dependent excretion pattern exists for dipyanone versus its metabolites, EMDPB and EMDPBA.

The N-demethylation of methadone to EDDP is primarily mediated by the cytochrome P450 (CYP) 2B6 isoenzyme (52) CYP2B6 expression is highly variable due to genetic polymorphisms and non-genetic factors such as induction or inhibition by xenobiotics (53). If CYP2B6 is also involved in dipyanone metabolism, its inhibition could increase the risk of dipyanone overdose. Additionally, inter-individual variability in CYP2B6 activity could lead to

significant differences in the urinary concentration ratios of dipyanone to EMDPB and EMDPBA. Further studies are needed to explore these metabolic dynamics and their clinical implications (44).

5.1.3. Protonitazepyne and Metonitazepyne metabolism

A strong correlation was observed between metabolites identified in protonitazepyne-positive real samples and those detected in human hepatocytes. The most abundant metabolites in both *in vitro* and *in vivo* settings included pyrrolidine ring opening to N-butanoic acid (B16), followed by oxidation (B17), O-dealkylation and O-glucuronidation (B2), and hydroxylation (B10) (45).

Metonitazepyne exhibited a similar metabolic profile, with the main transformations comprising pyrrolidine ring opening to N-butanoic acid (A13), oxidation (A17), hydroxylation (A12), and O-dealkylation and O-glucuronidation (A3). These findings align with Berardinelli et al. (33), who reported that N-piperidinyl etonitazene undergoes predominant piperidinyl moiety ring opening, emphasizing the significant influence of functional groups on metabolic pathways. Consistent with prior *in vivo* studies (6,13), O-dealkylated and O-glucuronide metabolites were most abundant in urine, while nitro-reduction and oxidation were more frequently observed in blood samples (29,33,39,43,54,55).

In vitro metabolism studies on other nitazenes derivatives have similarly identified O-dealkylation as the most prevalent metabolic transformation within this compound class (43,55).

Figure 23 illustrates the proposed metabolic pathways for both protonitazepyne and metonitazepyne.

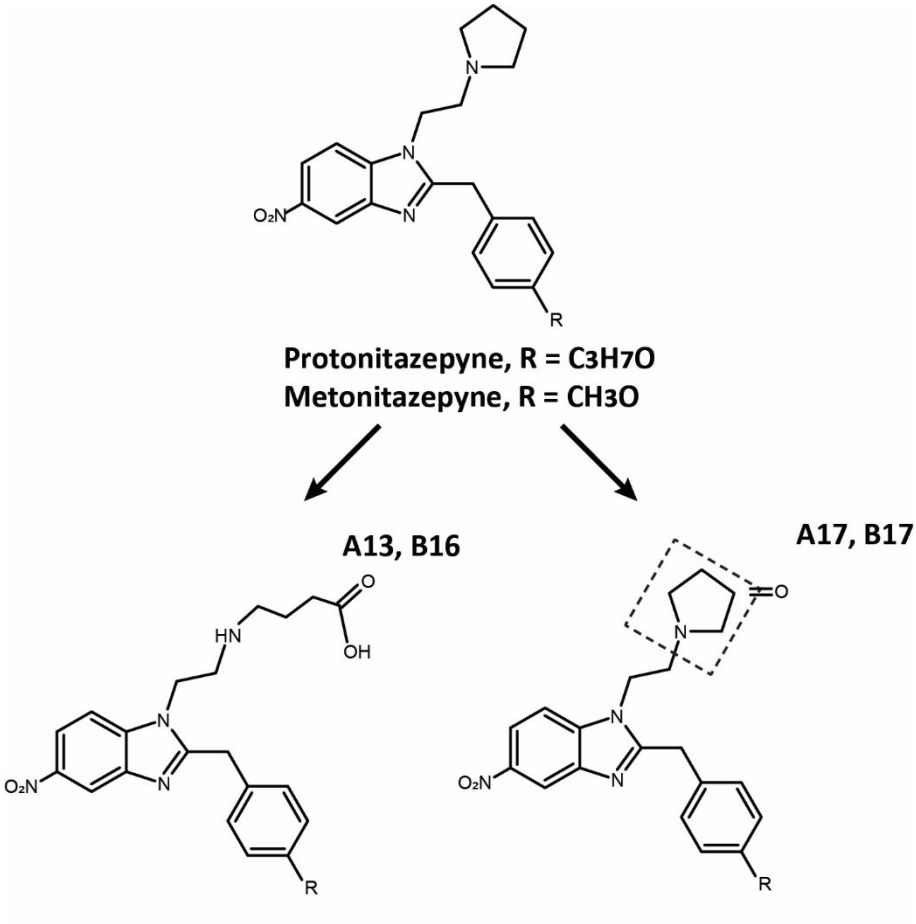


Figure 23: Proposed metabolic pathway for Protonitazepyne and Metonitazepyne

5.2. Pharmacological properties of nitazenes at opioid receptors

5.2.1. Etonitazepipne opioid receptors' activation

Etonitazepipne's pharmacological profile at MOR, DOR, and KOR was assessed using an HTRF based GTP Gi binding assay, revealing a potent activity at MOR with an EC_{50} of 9.4 nM, indicating significant affinity for this receptor. The efficacy at MOR was high, with an E_{max} of 143%, suggesting a strong activation of the receptor. At KOR, etonitazepine demonstrated a much lower potency with an EC_{50} of 3042 nM and a modest efficacy (E_{max} 13%), while at DOR, it showed an EC_{50} of

3215 nM and an E_{max} of 25%. These results indicate that etonitazepipne primarily exhibits high activity at MOR, with much weaker partial agonism at KOR and DOR, consistent with findings from other studies (19,39,50).

Published literature has consistently reported that etonitazepipne displays significant MOR activity, aligning with the current results, which show it as a potent MOR agonist with high efficacy. For instance, *in vivo* and *in vitro* studies have shown that etonitazepipne, like other nitazenes compounds, has a pharmacological profile that is strongly MOR-activation, which may contribute to its analgesic properties, but also its potential for respiratory depression and overdose risk (39). In comparison to fentanyl (EC_{50} 25.6 nM), etonitazepipne potency at MOR is around 3 times more potent, higher E_{max} (143%).

5.2.2. Dipyanone opioid receptors' activation

Dipyanone's pharmacological profile at MOR, DOR, and KOR was assessed using an HTRF based GTP Gi binding assay. Dipyanone exhibited significant potency at MOR, with an EC_{50} of 96 nM. While this is approximately four to five times lower than fentanyl (EC_{50}: 21 nM). These results suggest that dipyanone is a potent MOR agonist capable of inducing strong analgesic and euphoric effects, accompanied by risks of severe respiratory depression and dependency.

Comparison with earlier studies, such as those by Vandeputte et al. (15) confirmed similar trends in MOR activation. Despite methodological differences (EC_{50}: 39.9

nM vs. 96.8 nM in the present study), both studies corroborate that dipyanone is approximately four to five times less active than fentanyl at MOR.

At DOR, dipyanone demonstrated substantially lower potency and efficacy compared to the MOR findings. The compound exhibited an EC_{50} of 1070 nM and an E_{max} of 57%, markedly lower than the reference agonist SNC-80 (EC_{50}: 4.4 nM). These results are consistent with prior research, including findings by Charfi et al. (56) which affirm that dipyanone's activity at DOR is minimal.

Dipyanone's activity at KOR was also limited, with low potency (EC_{50}: 490 nM) and the lowest efficacy (E_{max}: 14%) among the investigated receptors. These values are significantly lower than those of the reference compound U-50488, whose results align with existing literature (26). The selective activation profile observed suggests that dipyanone has negligible agonist effects at KOR.

The selective receptor activation profile of dipyanone bears similarities to methadone, as both show strong MOR activity with relatively weak activity at DOR and KOR. Manuscript published by Bockmühl and Ehrhart (17)and Janssen and Jageneau (57) found that dipyanone's analgesic potency is approximately 5–10 times higher than pethidine and comparable to methadone in murine models. Similar LD50 values (~17 mg/kg) were reported for methadone and dipyanone in toxicity assessments conducted in mice (Scott et al., 1946, 1947).

Dipyanone exhibits a pharmacological profile consistent with strong MOR agonism, similar to methadone, which likely explains its potential for analgesia and euphoria as well as its associated risks, including respiratory depression and

dependency. Its weak activity at DOR and KOR further distinguishes its selective receptor engagement, reinforcing its similarity to methadone while highlighting its potent MOR-mediated effects.

5.2.3. Protonitazepyne and metonitazepyne opioid receptors' activation

The activation profiles of protonitazepyne and metonitazepyne at MOR, KOR, and DOR were evaluated using an HTRF®-based GTP Gi binding assay (45). Both compounds displayed significantly higher potency at MOR compared to fentanyl. Protonitazepyne was approximately 8–9 times more potent (EC50: 3.7 nM vs. 25.6 nM for fentanyl), while metonitazepyne was roughly 3 times more potent (EC50: 11.5 nM vs. 25.6 nM).

These findings align with data reported by De Vrieze et al. and Baumann et al. (19,50), which indicate that N-pyrrolidine substitutions, such as in protonitazepyne, metonitazepyne, etonitazepyne, correlate with increased MOR potency, displaying EC_{50} values ranging from 0.5–12 nM and 0.3–18 nM. In contrast, substitutions with an N-piperidinyl group result in reduced MOR potency. Similarly, the absence of a nitro group has also been associated with decreased potency (7,20,50).

Protonitazepyne exhibited an E_{max} of 154%, surpassing fentanyl's arbitrary maximum of 100%, indicating stronger MOR activation. Metonitazepyne's E_{max} was comparable to fentanyl at 101%.

Both compounds demonstrated minimal activity at KOR and DOR compared to reference agonists, suggesting weak partial agonism at these receptors.

At KOR, protonitazepyne showed low potency (EC_{50}: 2529.1 nM) and minimal efficacy (E_{max}: 14%). Metonitazepyne exhibited slightly greater potency (EC_{50}: 256.7 nM) and efficacy (E_{max}: 22%) compared to protonitazepyne. Despite these differences, both compounds displayed markedly lower activation at KOR compared to full agonists like U-50488.

At DOR, both compounds showed better activity than at KOR but remained less effective than SNC-80. Protonitazepyne exhibited an EC_{50} of 424.7 nM, while metonitazepyne was slightly more potent, with an EC_{50} of 265.8 nM. However, their efficacy at DOR was still limited, reinforcing their classification as weak partial agonists at this receptor.

These findings are consistent with previous studies, which have reported limited agonist activity of nitazene derivatives at KOR and DOR (50). However, receptor activation and efficacy are assay-dependent. The HTRF-based GTP Gi binding assay employed in this study may yield different results from other methodologies, such as the [35S]GTPγS binding assay. Minor assay variations can impact receptor activation characterization, underscoring the importance of contextual interpretation of efficacy data.

6. Conclusion

6.1. Key findings

This study has provided significant insights into the metabolism and pharmacological characterization of NSOs, specifically focusing on nitazenes and diphenylmethylpiperidine derivatives (33,44,45).

For the first time, *in vitro* and vivo metabolism, dipyanone, protonitazepyne, and metonitazepyne was characterized using cryopreserved primary human hepatocytes LC-HRMS-MS analysis and software-assisted data mining. Etonitazepipne metabolism was assessed through incubation with pHLMs, analysis with LC-HRMS-MS and software-assisted data mining.

Moreover, MOR, KOR and DOR activation was assessed providing critical information about their potency and efficacy through a novel high-throughput HTRF-based assay.

6.2. Implications

The study proposes valuable metabolite biomarkers that enable the prompt and accurate detection of NSOs in biological samples.

For etonitazepipne we propose as biomarker of consumption metabolite A10 (O-dealkylation) A5 (O-deethylation and ketone formation or N-Oxidation) and A17 (ring opening of a N-substituted piperidine).

For dipyanone, the primary metabolites identified were generated after pyrrolidine opening to butanol and butanoic acid followed by cyclisation (B12 and B13).

For protonitazepyne and metonitazepyne the proposed metabolites included C16 and D14 (ring opening to N-butanoic acid), C17 and D17 (oxidation) and C8 and D6 (O-dealkylation).

Additionally, the high-throughput, fast, and reliable HTRF-based activity assay developed in this study provides a crucial tool for the pharmacological profiling of emerging NSOs, paving the way for better understanding and managing their risks. As a result, protonitazepyne was the most potent and efficacious agonist at MOR, resulting around 6 times more potent than fentanyl, followed by etonitazepipne, metonitazepyne and dipyanone. This study underscores the critical need for comprehensive studies on these NSOs, along with their strong MOR agonist activity not only highlights their potential for severe analgesic effects but also for respiratory depression, overdose, and addiction risks. Understanding their metabolic and pharmacological profiles is essential to help forensic and analytical toxicologists for the detection of intoxication cases and for implementing effective public health measures to mitigate this growing threat.

6.3. Limitations and Future perspectives

The *in vitro* models, though effective, may not fully replicate the complexity of *in vivo* metabolic pathways due to inter individual genetic variability.

Considering the limited information about their metabolism, availability of authentic human samples is lacking.

Although, the study focused on a small panel of compounds, currently a wide panel of NSOs it has been investigated. Finally, it is important to note that different assay methods might yield in different receptor activation results, highlighting the critical need for the development of advanced and standardized assays allowing a precise characterization and risk assessment to address public health implications.

Acknowledgments

This study was conducted within the framework of the Italian "National plan to prevent misuse of fentanyl and other synthetic opioids", Chapter 6 "Preclinical evaluation of synthetic opioids' pharmaco-toxicological effects and interactions with new substances".

7. Bibliography

1. United Nations Office on Drugs and Crime (UNODC). Post-UNGASS 2016: NPS trends, challenges and recommendations 2016. Global smart update. 2016;16.
2. World Drug Report 2024 [Internet]. [cited 2024 Nov 26]. Available from: https://www.unodc.org/unodc/en/data-and-analysis/world-drug-report-2024.html
3. Opioids | National Institute on Drug Abuse (NIDA) [Internet]. [cited 2024 Nov 26]. Available from: https://nida.nih.gov/research-topics/opioids
4. Prekupec MP, Mansky PA, Baumann MH. Misuse of Novel Synthetic Opioids: A Deadly New Trend. J Addict Med [Internet]. 2017 [cited 2024 Nov 26];11(4):256–65. Available from: https://journals.lww.com/journaladdictionmedicine/fulltext/2017/08000/misuse_of_novel_synthetic_opioids__a_deadly_new.5.aspx
5. Bao Y, Meng S, Shi J, Lu L. Control of fentanyl-related substances in China. Lancet Psychiatry [Internet]. 2019 Jul 1 [cited 2024 Nov 26];6(7):e15. Available from: http://www.thelancet.com/article/S2215036619302184/fulltext
6. Office of the Federal Register NA and RA. Public Law 116 - 114 - Temporary Reauthorization and Study of the Emergency Scheduling of Fentanyl Analogues Act. govinfo.gov [Internet]. 2020 Feb 6 [cited 2024 Nov 26]; Available from: https%3A%2F%2Fwww.govinfo.gov%2Fapp%2Fdetails%2FPLAW-116publ114
7. Vandeputte MM, Van Uytfanghe K, Layle NK, St. Germaine DM, Iula DM, Stove CP. Synthesis, Chemical Characterization, and μ-Opioid Receptor Activity Assessment of the Emerging Group of “nitazene” 2-Benzylbenzimidazole Synthetic Opioids. ACS Chem Neurosci. 2021;12(7):1241–51.
8. European Monitoring Centre for Drugs and Drug Addiction. Report on the risk assessment of N,N-diethyl-2- [[4-(1-methylethoxy)phenyl]methyl]-5-nitro-1H-benzimidazole-1-ethanamine (isotonitazene) in accordance with Article 5c of Regulation (EC) No 1920/2006 (as amended). 2020;(31):55.
9. Hunger A, Kebrle J, Rossi A, Hoffmann K. Synthese basisch substituierter, analgetisch wirksamer Benzimidazol-Derivate. Experientia. 1957;13(10):400–1.
10. Hunger A, Kebrle J, Rossi A, Hoffman K. Benzimidazol-Derivate und verwandte Heterocyclen III. Synthese von 1-Aminoalkyl-2-benzyl-nitro-benzimidazol. Helv Chim Acta. 1960;43(4):941–1164.
11. Ujváry I, Christie R, Evans-Brown M, Gallegos A, Jorge R, De Morais J, et al. DARK Classics in Chemical Neuroscience: Etonitazene and Related Benzimidazoles. Vol. 12, ACS Chemical Neuroscience. 2021. p. 1072–92.
12. Montanari E, Madeo G, Pichini S, Busardò FP, Carlier J. Acute Intoxications and Fatalities Associated with Benzimidazole Opioid (Nitazene Analog) Use: A Systematic Review. Ther Drug Monit. 2022;494–510.

13. EMCDDA. European Monitoring Centre for Drugs and Drug Addiction (2024), European Drug Report 2024: Trends and Developments,. 2024.

14. European Monitoring Centre for Drugs and Drug Addiction. European Drug Report 2023: Trends and Developments [Internet]. 2023. Available from: https://www.emcdda.europa.eu/publications/european-drug-report/2023_en

15. Vandeputte MM, Walton SE, Shuda SA, Papsun DM, Krotulski AJ, Stove CP. Detection, chemical analysis, and pharmacological characterization of dipyanone and other new synthetic opioids related to prescription drugs. Anal Bioanal Chem. 2023 Sep 1;415(21):5165–80.

16. Scott CC, Robbins EB, Chen KK. Comparison of some new analgesic compounds. Science (1979) [Internet]. 1946 Dec 20 [cited 2024 Jun 11];104(2712):587–8. Available from: https://www.science.org/doi/10.1126/science.104.2712.587

17. Bockmühl M, Ehrhart G. Über eine neue Klasse von spasmolytisch und analgetisch wirkenden Verbindungen, I. Justus Liebigs Ann Chem [Internet]. 1949 Jan 1 [cited 2024 Jun 11];561(1):52–86. Available from: https://onlinelibrary.wiley.com/doi/full/10.1002/jlac.19495610107

18. European Database on New Drugs. EUDA [Internet]. 2023 [cited 2024 Jul 25]. Available from: https://ednd2.emcdda.europa.eu/ednd/

19. De Vrieze LM, Walton SE, Pottie E, Papsun D, Logan BK, Krotulski AJ, et al. In vitro structure-activity relationships and forensic case series of emerging 2-benzylbenzimidazole “nitazene” opioids. Arch Toxicol [Internet]. 2024 Sep 1 [cited 2024 Sep 26];98(9):2999–3018. Available from: https://pubmed.ncbi.nlm.nih.gov/38877156/

20. Monti MC, De Vrieze LM, Vandeputte MM, Persson M, Gréen H, Stove CP, et al. Detection of N-desethyl etonitazene in a drug checking sample: Chemical analysis and pharmacological characterization of a recent member of the 2-benzylbenzimidazole “nitazene” class. J Pharm Biomed Anal [Internet]. 2024 Dec 15 [cited 2024 Sep 26];251. Available from: https://pubmed.ncbi.nlm.nih.gov/39216307/

21. Lambert DG. Opioids and opioid receptors; understanding pharmacological mechanisms as a key to therapeutic advances and mitigation of the misuse crisis. BJA Open [Internet]. 2023 Jun 1 [cited 2024 Nov 26];6:100141. Available from: http://www.bjaopen.org/article/S2772609623000205/fulltext

22. Paul AK, Smith CM, Rahmatullah M, Nissapatorn V, Wilairatana P, Spetea M, et al. Opioid analgesia and opioid-induced adverse effects: A review. Pharmaceuticals. 2021 Nov 1;14(11).

23. Stein C. Opioid receptors. Annu Rev Med. 2016 Jan 14;67:433–51.

24. James A, Williams J. Basic Opioid Pharmacology — An Update. Br J Pain. 2020 May 1;14(2):115–21.

25. Koval A, Kopein D, Purvanov V, Katanaev VL. Europium-labeled GTP as a general nonradioactive substitute for [35S]GTPγS in high-throughput G protein studies. Anal Biochem. 2010 Feb 15;397(2):202–7.

26. Otte L, Wilde M, Auwärter V, Grafinger KE. Investigation of the μ- and κ-opioid receptor activation by eight new synthetic opioids using the [35S]-GTPγS assay: U-47700, isopropyl U-47700, U-49900, U-47931E, N-methyl U-47931E, U-51754, U-48520, and U-48800. Drug Test Anal. 2022 Jul 1;14(7):1187–99.

27. Rozwandowicz-Jansen A, Laurila J, Martikkala E, Frang H, Hemmilä I, Scheinin M, et al. Homogeneous GTP binding assay employing QRET technology. J Biomol Screen [Internet]. 2010 [cited 2024 Oct 18];15(3):261–7. Available from: https://pubmed.ncbi.nlm.nih.gov/20103692/

28. Montanari E, Madeo G, Pichini S, Busardò FP, Carlier J. Acute Intoxications and Fatalities Associated With Benzimidazole Opioid (Nitazene Analog) Use: A Systematic Review. Ther Drug Monit. 2022 Aug 1;44(4):494–510.

29. Taoussi O, Berardinelli D, Zaami S, Tavoletta F, Basile G, Kronstrand R, et al. Human metabolism of four synthetic benzimidazole opioids: isotonitazene, metonitazene, etodesnitazene, and metodesnitazene. Arch Toxicol. 2024 Jul 1;98(7):2101–16.

30. De Bruyn Kops C, Šícho M, Mazzolari A, Kirchmair J. GLORYx: Prediction of the Metabolites Resulting from Phase 1 and Phase 2 Biotransformations of Xenobiotics. Chem Res Toxicol [Internet]. 2021 Feb 15 [cited 2022 Oct 3];34(2):286–99. Available from: https://pubs.acs.org/doi/full/10.1021/acs.chemrestox.0c00224

31. Bruyn Kops C de, Šícho M, Mazzolari A, Kirchmair J. GLORYx: Prediction of the Metabolites Resulting from Phase 1 and Phase 2 Biotransformations of Xenobiotics. Chem Res Toxicol [Internet]. 2020 Feb 15 [cited 2021 Sep 21];34(2):286–99. Available from: https://pubs.acs.org/doi/abs/10.1021/acs.chemrestox.0c00224

32. Brunetti P, Berardinelli D, Giorgetti A, Schwelm HM, Haschimi B, Pelotti S, et al. Human metabolism and basic pharmacokinetic evaluation of AP-238: A recently emerged acylpiperazine opioid. Drug Test Anal. 2023;

33. Berardinelli D, Taoussi O, Carlier J, Tini A, Zaami S, Sundermann T, et al. In vitro, in vivo metabolism and quantification of the novel synthetic opioid N-piperidinyl etonitazene (etonitazepipne). Clin Chem Lab Med [Internet]. 2024 Jul 1 [cited 2024 Sep 26];62(8):1580–90. Available from: https://www.degruyter.com/document/doi/10.1515/cclm-2023-1360/html

34. Manier SK, Valdiviezo JA, Eckstein N, Meyer MR. Investigations on the in vitro and in vivo metabolic fate of the new synthetic opioid desmethylmoramide using HPLC-HRMS/MS for toxicological screening purposes. Drug Test Anal [Internet]. 2024 Mar 1 [cited 2024 Oct 31];16(3):309–13. Available from: https://pubmed.ncbi.nlm.nih.gov/37464572/

35. Ferrari A, Coccia CPR, Bertolini A, Sternieri E. Methadone - Metabolism, pharmacokinetics and interactions. Pharmacol Res [Internet]. 2004 Dec [cited 2024 Oct 18];50(6):551–9. Available from: https://pubmed.ncbi.nlm.nih.gov/15501692/

36. Krotulski AJ, Papsun DM, Walton SE, Logan BK. Metonitazene in the United States — Forensic toxicology assessment of a potent new synthetic opioid using liquid chromatography mass spectrometry. 2021;(June):1697–711.

37. Krotulski AJ, Papsun DM, Kacinko SL, Logan BK. Isotonitazene Quantitation and Metabolite Discovery in Authentic Forensic Casework. J Anal Toxicol [Internet]. 2021 [cited 2022 Jul 1];44(6):521–30. Available from: https://pubmed.ncbi.nlm.nih.gov/32091095/

38. Krotulski A, Papsun DM, Walton SE, Logan BK. New High Potency Synthetic Opioid N-Pyrrolidino Etonitazene (Etonitazepyne) Linked to Overdoses Across United States. 2021; Available from: www.npsdiscovery.org

39. Vandeputte MM, Verougstraete N, Walther D, Glatfelter GC, Malfliet J, Baumann MH, et al. First identification, chemical analysis and pharmacological characterization of N-piperidinyl etonitazene (etonitazepipne), a recent addition to the 2-benzylbenzimidazole opioid subclass. Arch Toxicol [Internet]. 2022;96(6):1865–80. Available from: https://doi.org/10.1007/s00204-022-03294-2

40. Keller BO, Sui J, Young AB, Whittal RM. Interferences and contaminants encountered in modern mass spectrometry. Anal Chim Acta. 2008;627(1):71–81.

41. Krotulski AJ, Papsun DM, Noble C, Kacinko SL, Logan BK. Brorphine—Investigation and quantitation of a new potent synthetic opioid in forensic toxicology casework using liquid chromatography-mass spectrometry. J Forensic Sci [Internet]. 2021 Mar 1 [cited 2022 Jul 1];66(2):664–76. Available from: https://pubmed.ncbi.nlm.nih.gov/33201526/

42. Calello D, Aldy K, Jefri M, Nguyen TAT, Krotulski AJ, Logan BK. Identification of a novel opioid, N-piperidinyl etonitazene (etonitazepipne), in patients with suspected opioid overdose. Clin Toxicol. 2022;60(9):1067.1069.

43. Ameline A, Gheddar L, Pichini S, Stove C, Aknouche F, Maruejouls C, et al. In vitro characterization of protonitazene metabolites, using human liver microsomes, and first application to two urines collected from death cases. Clin Chim Acta [Internet]. 2024 Jul 15 [cited 2024 Sep 26];561. Available from: https://pubmed.ncbi.nlm.nih.gov/38844019/

44. Berardinelli D, Kutzler J, Taoussi O, Zaami S, Pichini S, Basile G, et al. Dipyanone, a new methadone-like synthetic opioid: In vitro and in vivo human metabolism and pharmacological profiling. Manuscript Under Review. 2024;

45. Berardinelli D, Taoussi O, Ovat Y, Pichini S, Auwärter V, Pulver B, et al. Computational analysis, pharmacological characterization, in vitro and in vivo human metabolism of N-Pyrrolidino Nitazenes: Protonitazepyne and Metonitazepyne. Manuscript Under Review. 2024;

46. Di Trana A, La Maida N, Froldi R, Scendoni R, Busardò FP, Pichini S. The new synthetic benzimidazole opioid etonitazepipne: An emerging fatal harm and a challenge for laboratory medicine. Clin Chem Lab Med [Internet]. 2023 Apr 18 [cited 2023 Aug 8]; Available from: https://www.degruyter.com/document/doi/10.1515/cclm-2023-0186/html

47. Pohland A, Boaz HE, Sullivan HR. Synthesis and Identification of Metabolites Resulting from the Biotransformation of DL-Methadone in Man and in the Rat. J Med Chem [Internet]. 1971 Mar 1 [cited 2024 Oct 18];14(3):194–7. Available from: https://pubs.acs.org/doi/abs/10.1021/jm00285a004

48. Overman LE, Ricca DJ. The Intramolecular Mannich and Related Reactions. Comprehensive Organic Synthesis. 1991 Jan 1;1007–46.

49. Dilmaghanian S, Gerber JG, Filler SG, Sanchez A, Gal J. Enantioselectivity of inhibition of cytochrome P450 3A4 (CYP3A4) by ketoconazole: Testosterone and methadone as substrates. Chirality [Internet]. 2004 Jan 1 [cited 2024 Oct 18];16(2):79–85. Available from: https://onlinelibrary.wiley.com/doi/full/10.1002/chir.10294

50. Kozell LB, Eshleman AJ, Wolfrum KM, Swanson TL, Bloom SH, Benware S, et al. Pharmacologic Characterization of Substituted Nitazenes at μ, κ, and Δ Opioid Receptors Suggests High Potential for Toxicity. Journal of Pharmacology and Experimental Therapeutics [Internet]. 2024 May 1 [cited 2024 Sep 26];389(2):219–28. Available from: https://jpet.aspetjournals.org/content/389/2/219

51. Bernard JP, Opdal MS, Karinen R, Mørland J, Khiabani HZ. Relationship between methadone and EDDP (2-ethylidene-1,5-dimethyl-3,3- diphenylpyrrolidine) in urine samples from Norwegian prisons. Eur J Clin Pharmacol. 2007;63(8):777–82.

52. Kreutzwiser D, Tawfic QA. Methadone for Pain Management: A Pharmacotherapeutic Review. CNS Drugs [Internet]. 2020;34(8):827–39. Available from: https://doi.org/10.1007/s40263-020-00743-3

53. Zanger UM, Klein K. Pharmacogenetics of cytochrome P450 2B6 (CYP2B6): Advances on polymorphisms, mechanisms, and clinical relevance. Front Genet. 2013;4(MAR):1–12.

54. Vandeputte MM, Krotulski AJ, Walther D, Glatfelter GC, Papsun D, Walton SE, et al. Pharmacological evaluation and forensic case series of N-pyrrolidino etonitazene (etonitazepyne), a newly emerging 2-benzylbenzimidazole 'nitazene' synthetic opioid. Arch Toxicol [Internet]. 2022 Jun 1 [cited 2022 Jun 19];96(6):1845–63. Available from: https://pubmed.ncbi.nlm.nih.gov/35477798/

55. Murari M, Pesavento S, Greco F, Vettori A, Tagliaro F, Gottardo R. Study of metabolism and potential toxicity of nine synthetic opioid analogs using the zebrafish larvae model. Drug Test Anal [Internet]. 2024 Jun 1 [cited 2024 Sep 26];16(6):629–37. Available from: https://pubmed.ncbi.nlm.nih.gov/37916273/

56. Charfi I, Nagi K, Mnie-Filali O, Thibault D, Balboni G, Schiller PW, et al. Ligand- and cell-dependent determinants of internalization and cAMP modulation by delta opioid receptor (DOR) agonists. Cellular and Molecular Life Sciences. 2014;71(8):1529–46.

57. Janssen PAJ, Jageneau AH. A New Series of Potent Analgesics. Journal of Pharmacy and Pharmacology [Internet]. 2011 Apr 12 [cited 2024 Jun 11];9(1):381–400. Available from: https://dx.doi.org/10.1111/j.2042-7158.1957.tb12290.x